Supporting Information for

Structural variety of 5-fluoroarene-2-aminopyrimidine in comparison to 2-aminopyrimidine silver(I) coordination polymers: progress report and overview

Jens Eberhard,*[a] Ion Stoll,[a] Regina Brockhinke,[b] Beate Neumann,[c] Hans-Georg Stammler,[c] Arthur Riefer,[d] Eva Rauls,[d] Wolf Gero Schmidt,[d] and Jochen Mattay*[a]

[a] *Organische Chemie I, Fakultät für Chemie, Universität Bielefeld, Universitätsstr. 25, 33501 Bielefeld, Germany. Fax: +49 521 106 6417; Phone: +49 521 106 2072; E-mail: mattay@uni-bielefeld.de, jens.eberhard@uni-bielefeld.de*
[b] *Physikalische Chemie I, Fakultät für Chemie, Universität Bielefeld, Universitätsstr. 25, 33501 Bielefeld, Germany.*
[c] *Abteilung für Röntgenstrukturanalyse, Fakultät für Chemie, Universität Bielefeld, Universitätsstr. 25, 33501 Bielefeld, Germany.*
[d] *Lehrstuhl für Theoretische Physik, Universität Paderborn, Warburger Str. 100, 33095 Paderborn, Germany.*

Contents

Photographs of 11

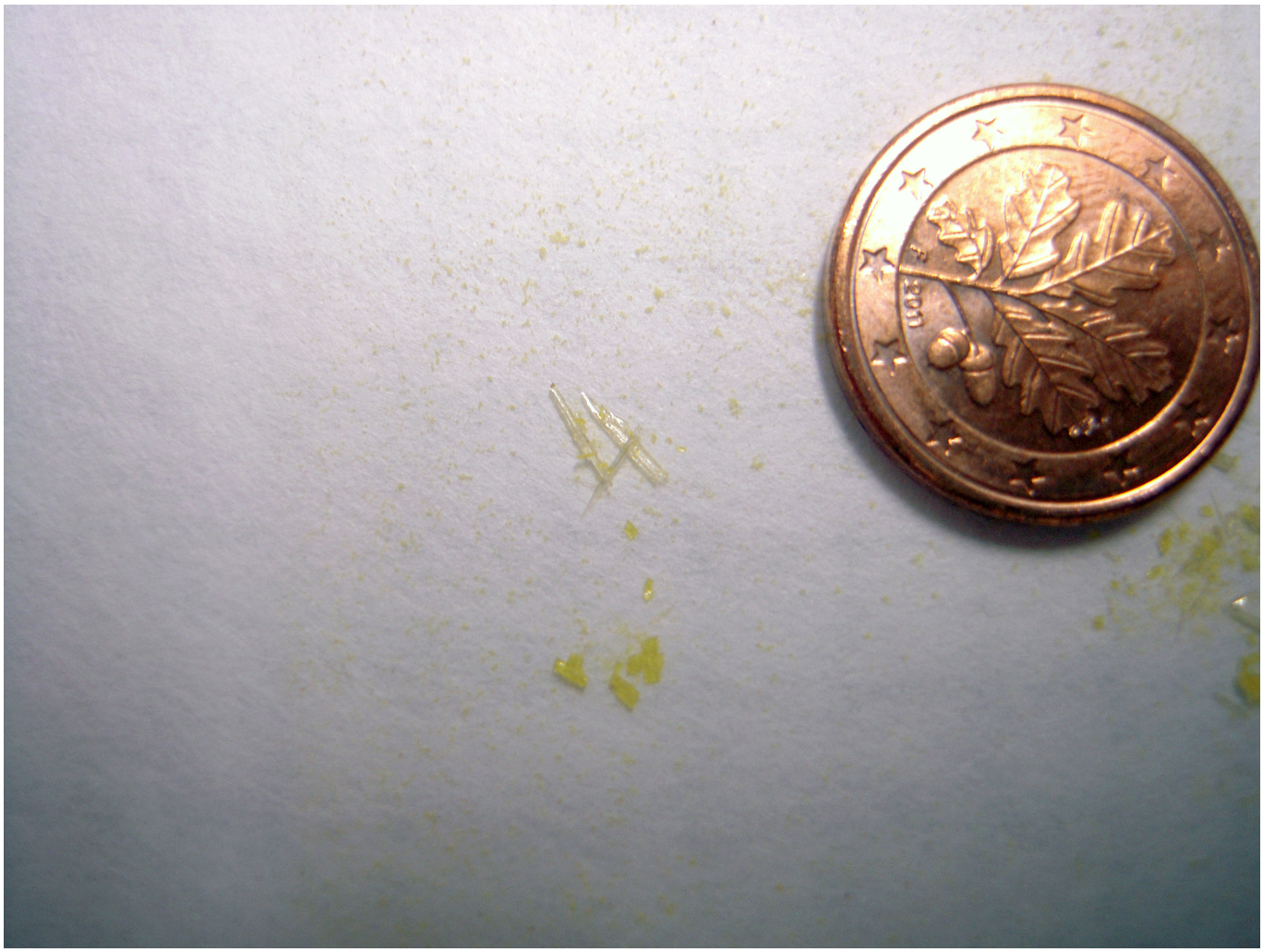

Fig. S 1 Photograph of crystals of **11a** and **11b** grew in one batch and size comparison by a 2-Cent coin (18.75 mm).

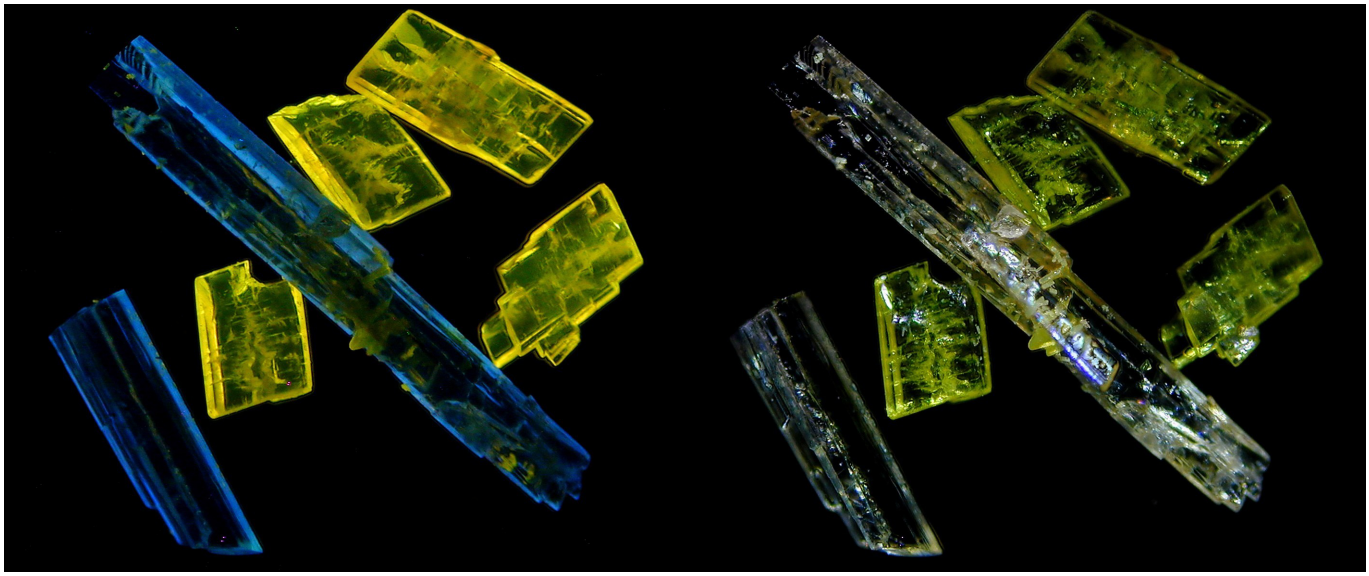

Fig. S 2 Microscopic photographs of crystals of **11a** and **11b** (see TOC picture) under Vis light illumination (by the microscope light source) and UV light (by a cold cathode tube or UV-LED) with UG11 optical glass filter used to bandpass the UV excitation and a GG435 optical glass filter for the emission light. One can notice that crystals of **11b** grew also on top of **11a**.

Experimental

Materials and Methods

Chemicals

Pentafluorophenyl acetic acid (99%, Acros Organics, Apollo Scientific or ABCR), sodium methoxide solution (25% in methnaol, Sigma-Aldrich) and aqueous dimethylamine solution (for synthesis, Merck) were used as received. All other chemicals and solvents used in the synthesis were of analytical grade and used without further purification. Silver salts were used as received: Silver nitrate (99%, Carl Roth), silver perchlorate anhyd. (48% Ag, ABCR), Silver *p*-toluenesulfonate (97%, Merck), silver trifluoromethanesulfonate (98%, Fluka; 99%, Apollo Scientific; Sigma-Aldrich), silver trifluoroacetate (99%, ABCR; 48.3% Ag, Fluka). Absolute ethanol (HPLC grade, VWR), anthracene (99%, Fluka), and 9,10-diphenylanthracene (99%, Acros Organics) were used for spectroscopy. 2-Aminopyrimidine (97%, Sigma-Aldrich, Lot 33821-465; 98%, Alfa Aesar, Lot 10154586; 98%, Acros Organics, Lot A0290607) was recrystallized from chloroform twice giving colorless plates. Mp. 126-127 °C (Lit.[1] 126-127 °C). A small sample of this material was furthermore also sublimed at 100 °C and $1{\cdot}10^{-3}$ mbar and checked against a recrystallized sample with no difference.

UV-Vis and photoluminescence (PL) spectra:

For all measurements, liquid samples were contained in quartz cuvettes of 10×10 mm^2 and solid samples were prepared on quartz plates. Absorption is measured with a ShimadzuUV-2550 or a Perkin Elmer Lambda 40 UV-VIS double beam spectrometer using the solvent as a reference. The setup used to acquire excitation-emission spectra (EES) was similar to that employed in commercial static fluorimeters: the output of a continuous 75 W Xe-lamp was wavelength-separated by a first monochromator and then used to irradiate a sample. The fluorescence was collected by mirror optics at right angles and imaged on the entrance slit of a second spectrometer while compensating astigmatism at the same time. The signal was detected by a back-thinned CCD camera (Roper Scientific) in the exit plane of the spectrometer. Details of this method can be found elsewhere.[2] Routine fluorescence measurements (*cf.* on liquid samples) were also done on a Perkin Elmer LS 50B bench-top fluorescence spectrometer (slit width set to 5 nm).

Elemental analyses

C, H, and N analyses were carried out by the in-house microanalytical service on a EuroEA CHN analyzer (HEKAtech GmBH).

NMR

NMR spectra were recorded on a Bruker DRX 500 (^{1}H operating at 500.13 MHz) or on a Bruker Avance AV300 (^{1}H operating at 300.13 MHz). All spectra were referenced on the residual proton solvent signal for ^{1}H or ^{13}C spectra (*cf.* DMSO-d_6 2.500 ppm; 39.52 ppm). ^{1}F NMR measurements on the DRX500 were referenced against a external standard (parameter stored), for measurements on the AV300 a internal standard ($CFCl_3$) in a sealed capillary was used.

IR

IR spectra were recorded on a Nicolet 380 (Thermo Scientific, Firmware 2.11) FT-IR with Smart Orbit Diamond ATR cell. Data processing was done by using the OMNIC Software 7.3. Resolution was set to 2.00 cm^{-1}. Strong bands are therefore considered to be accurate to 2 cm^{-1} but weak bands are less reliable.

Synthesis of the ligands

5-(2,3,4,5,6-Pentafluoro-phenyl)-pyrimidin-2-ylamine (FAP, 1):

Pentaflouro-2-aminopyrimidine (FAP, **1**) was synthesized as described previously.[3¶] Partial deuteration was archived by stirring a small amount (65 mg) in MeOH-d4 (15 ml) with 0.1 ml D_2O and 5 drops TFA-d1 under reflux (for solubility reasons) for 2 h.

¶It was noted if the reaction is run too long some –NMe_2 substitution already occurred. Application of slight *vacuo* did not solve this issue. Therefore, such batches were preferably converted to the NFAP ligand.

A NMR sample of this mixture showed complete loss of the $-NH_2$ resonance (Figure S5) and no indication of substitution of the *para*-fluoro atom by MeOH-d4 in the ^{19}F NMR spectra (Figure S6). Evaporation of the solvent gave the FAP-d2 derivative, which was quickly mounted to the IR ATR setup. A second NMR (in DMSO-d6, Figure S5) shortly after the measurement showed already *ca.* 80% recovery of the $-NH_2$ resonance by proton exchange with atm. moisture and residual water.

5-(2,3,5,6-Tetrafluoro-4-methoxyphenyl)-pyrimidin-2-ylamine (OFAP, 2):

A solution of about 20 equivalents excess sodium methoxid was prepared by either dissolving an appropriate amount sodium under reflux in methanol or using a commercial 25% sodium methoxide solution directly and dilute this by four parts methanol. FAP **1** (e.g. 205 mg (0.79 mmol)) was added and the solution was heated to reflux overnight.‖ The solvent was evaporated in vacuo and the remaining solid was suspended in 25% NH_4Cl soln. under sonication (e.g. about 50 mL) resulting in a about pH 8 suspension. The suspension was filtered through a fritted glass Büchner funnel to give the crude product in 96% yield and 95% purity by NMR. Last traces of FAP could be removed by (repeated) recrystallization of the remaining solid from ethanol (*ca.* 90 mL) to afford typically 60-86% OFAP **2** as colourless solid (e.g. 185 mg, 0.67 mmol, 86%). M.p.: 261 °C. ^{1}H NMR (500 MHz, DMSO-d_6): δ = 8.35 (s, 2 H, ArH), 7.09 (2 H, s, NH_2), 4.08 (s, 3 H, OCH_3) ppm. ^{19}F NMR (470 MHz, DMSO-d_6): δ = -145.9 (dd, $^3J_{(F,F)}$ = 23.8 Hz, $^4J_{(F,F)}$ = 8.3 Hz), -158.6 (dd, $^3J_{(F,F)}$ = 23.8 Hz, $^4J_{(F,F)}$ = 8.3 Hz) ppm. ^{13}C NMR (125 MHz, 50°C** DMSO-d_6): δ = 163.1, 158.3, 143.7 (dt, $^1J_{(C,F)}$ = 243.0 Hz, $^2J_{(C,F)}$ = 10.3 Hz), 140.5 (dd, $^1J_{(C,F)}$ = 246.0 Hz, $^2J_{(C,F)}$ = 15.5 Hz), 136.7 (t, $^2J_{(C,F)}$ = 10.4 Hz), 109.2, 108.9 (t, $J_{(C,F)}$ = 17.8 Hz,), 62.1 ppm. IR (ATR): 3351, 3294, 3156, 2968, 2735, 1747, 1691, 1652, 1610, 1545, 1480, 1428, 1392, 1378, 1226, 1096, 1037, 981, 950, 935, 845, 799, 777, 656, 640, 544, 496, 449, 439 cm^{-1}. HRMS (ESI): m/z calcd. for $C_{11}H_8F_4N_3O$ $[M+H]^+$: 274.05980; found 274.05956. Requires C 48.36, H 2.58, N 15.38; anal. found: C 49.10, H 2.64, N 15.11%.

5-(4-(Dimethylamino)-2,3,5,6-tetrafluorophenyl)-pyrimidin-2-amine (NFAP, 3):

Small scale: 170 mg (0.65 mmol) of FAP **1** was dissolved in 30 mL DMSO and 9 mL of dimethylamine in water (40%). The reaction mixture was heated in a heavy wall Pyrex srew cap tube for 3 h to 120 °C and given on 75 mL 25% NH_4Cl solution. The resulting precipitate was filtered off and recrystallized from ethanol to afford 147 mg (0.51 mmol, 78%) NFAP **3** as colourless solid.

Prep. scale: 2.67 g (10.2 mmol) **1** was dissolved in 60 mL DMSO and 20 mL aqueous dimethylamine (40%) by heating to 120 °C and stirred at his temperature for 21 h stoppered by an rubber balloon (filled with Argon). **3** precipitates up on cooling at this concentration and was subsequently isolated by filtration as above and washed with *ca.* 200 mL water (in portions). Drying gave 2.31 g (8.0 mmol, 78%) **3** as colorless solid. M.p.: 259 °C. ^{1}H NMR (500 MHz, DMSO-d_6): δ = 8.33 (s, 2 H, ArH), 7.05 (2 H, s, NH_2), 2.94 (s, 6 H, $N(CH_3)_2$) ppm. ^{19}F NMR (470 MHz, 50°C†† DMSO-d_6): δ = -146.9 (dd, $^3J_{(F,F)}$ = 22.1 Hz, $^4J_{(F,F)}$ = 7.9 Hz), -152.3 (m) ppm. ^{13}C NMR (125 MHz, DMSO-d_6): δ = 163.1, 158.5, 145.0-140.5 (m), 130.7 (t, $^2J_{(C,F)}$ = 12.1 Hz), 109.8, 107.0 (t, $^3J_{(C,F)}$ = 18.2 Hz,), 42.9 ppm. IR (ATR): 3347, 3290, 3140, 2992, 2934, 2895, 2881, 2849, 2810, 2746, 1672, 1608, 1477, 1428, 1391, 1376, 1212, 1065, 1036, 974, 952, 898, 823, 804, 778, 732, 655, 570, 541, 497, 455, 434 cm^{-1}. HRMS (ESI): m/z calcd. for $C_{12}H_{11}F_4N_4$ $[M+H]^+$: 287.09144; found 287.09144. Requires C 50.35, H 3.52, N 19.57; anal. found C 50.37, H 3.39, N 18.95%.

Spectroscopic data of ligands

NMR data

5-Fluoroarene-2-aminopyrimidines **1** - **3** can be easily distinguished by ^{19}F NMR (Figure S 4). The fluorine atoms in 3,5-position on the fluoroarene part shift 4.86 ppm downfield for OFAP **2** compared to FAP **1** and additional 6.39 ppm for NFAP respectively, while there is a slight upfield shift for the *ortho* 2,6-F atoms of 1.76 ppm (OFAP; and further 0.98 ppm for NFAP) induced by

‖Good conversation was noticed after a few hours, however the ligands are not distinguishable by TLC (e.g. SiO_2, Cyhex/EtOAc 50:50) and so far, not even by HPLC (SiO_2, gradient Cyhex/EtOAc 33:66 → 0:100) where only NFAP gives a separated peak. However, GC or on-line ^{19}F NMR spectroscopy work well for monitoring.

**Higher temperature was necessary for solubility reasons.

the perturbation of electron density through the substituent in *para*-position. In contrast differentiation of the compounds by ^{1}H NMR is hardly possible in the downfield region of the spectra and only the introduced functional group itself gives rise to signals for identification (Figure S 3).

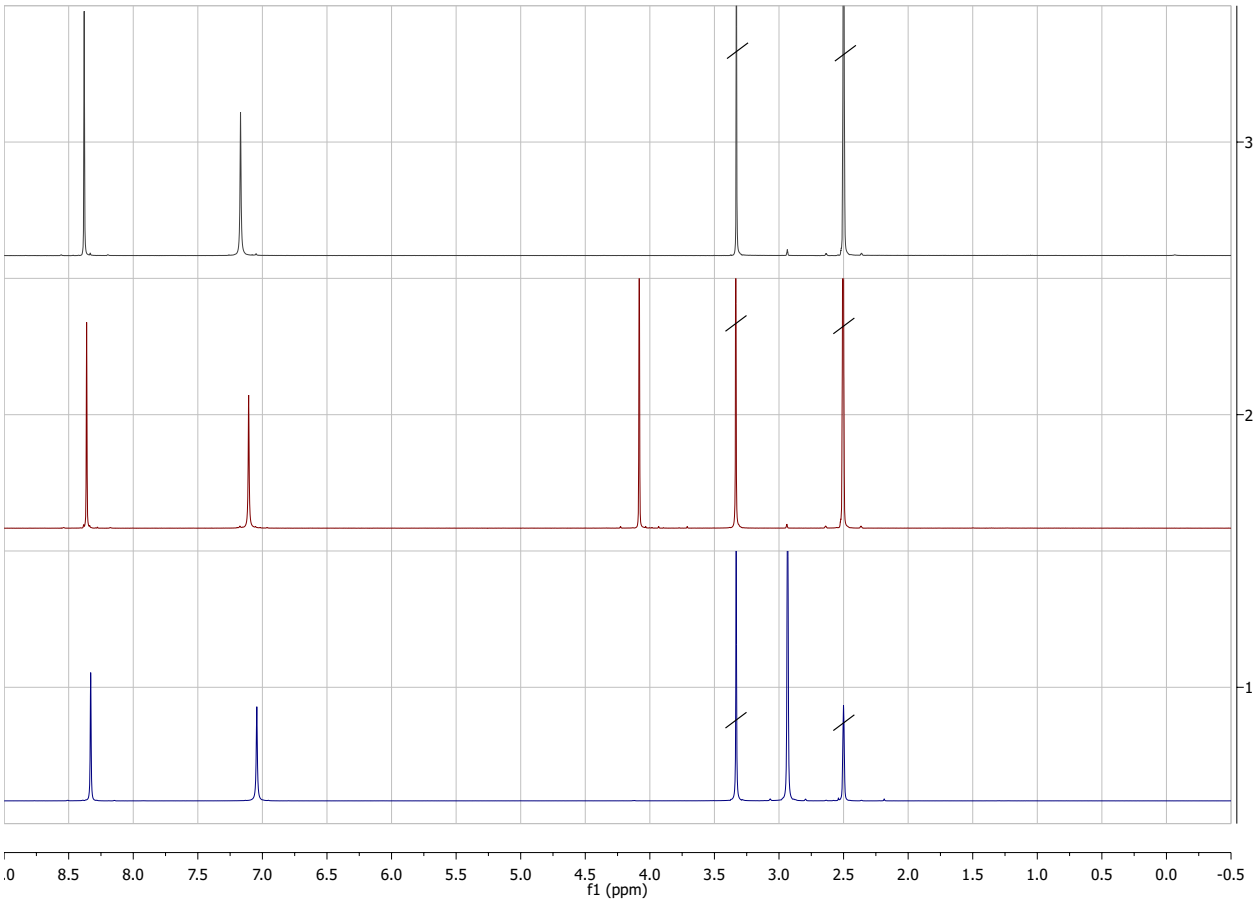

Fig. S 3 ^{1}H NMR data of FAP (anthracite black), OFAP (maroon red) and NFAP (navy blue) on a 500 MHz NMR spectrometer.

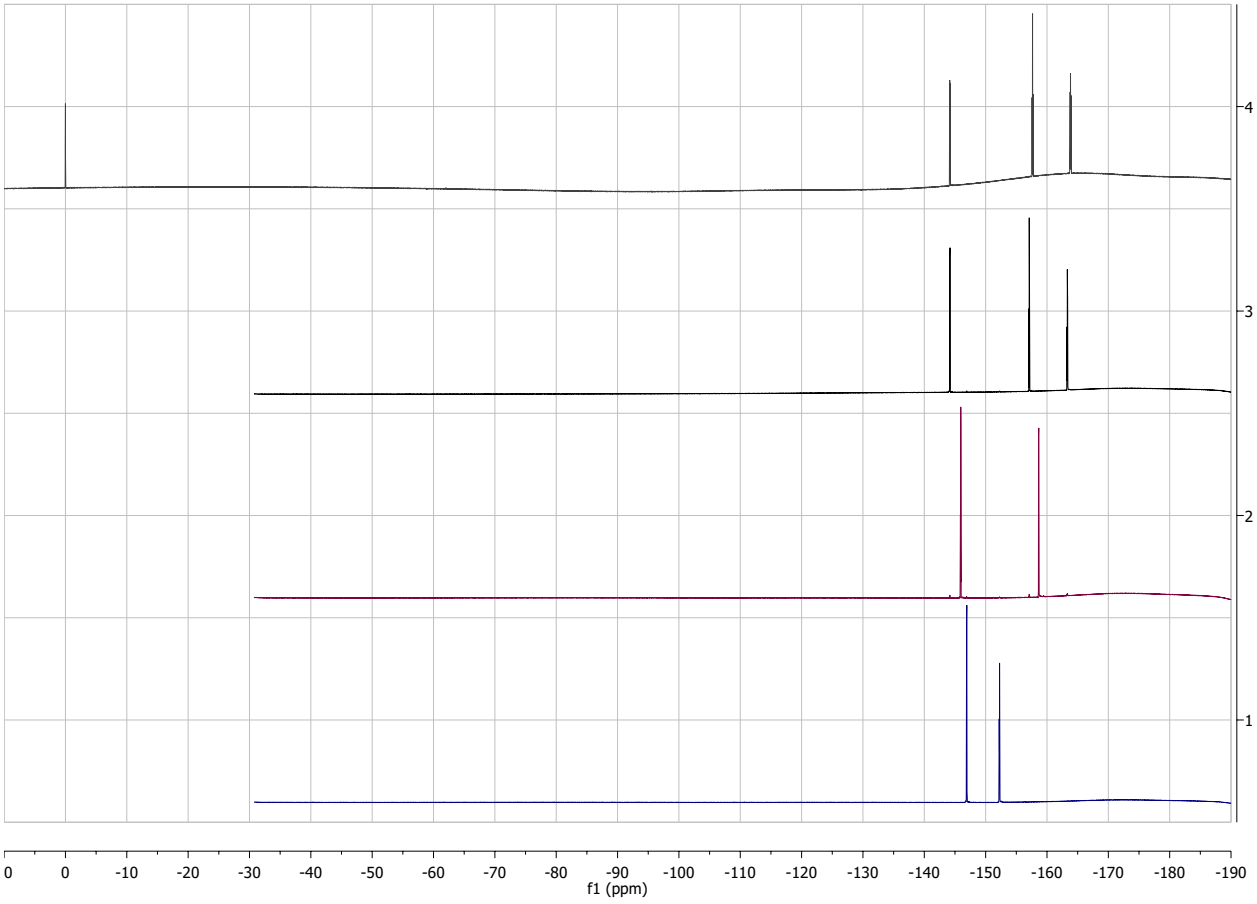

Fig. S 4 ^{19}F NMR data measured on a 300 MHz NMR spectrometer with $CFCl_3$ as internal standard (in capillary) and a different batch FAP (anthracite black) as well as OFAP (maroon red) and NFAP (navy blue) on a 500 MHz machine with external ^{19}F calibration.

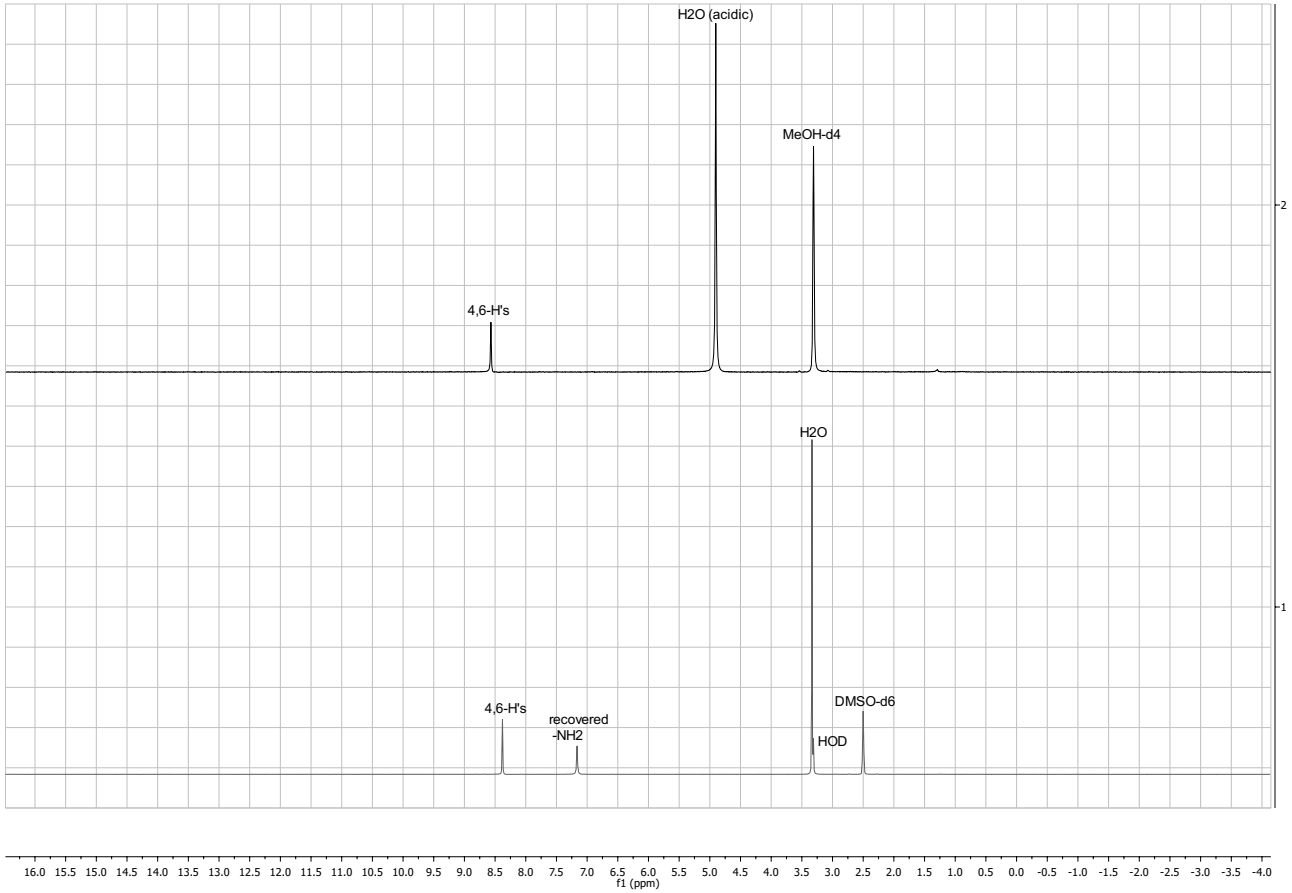

Fig. S 5 ^{1}H NMR data of deuterated FAP-d2 (black) and FAP (dark grey) in different solvents (MeOH-d_4 and a small amount TFA-d_1 (top) and DMSO-d_6 (bottom)).

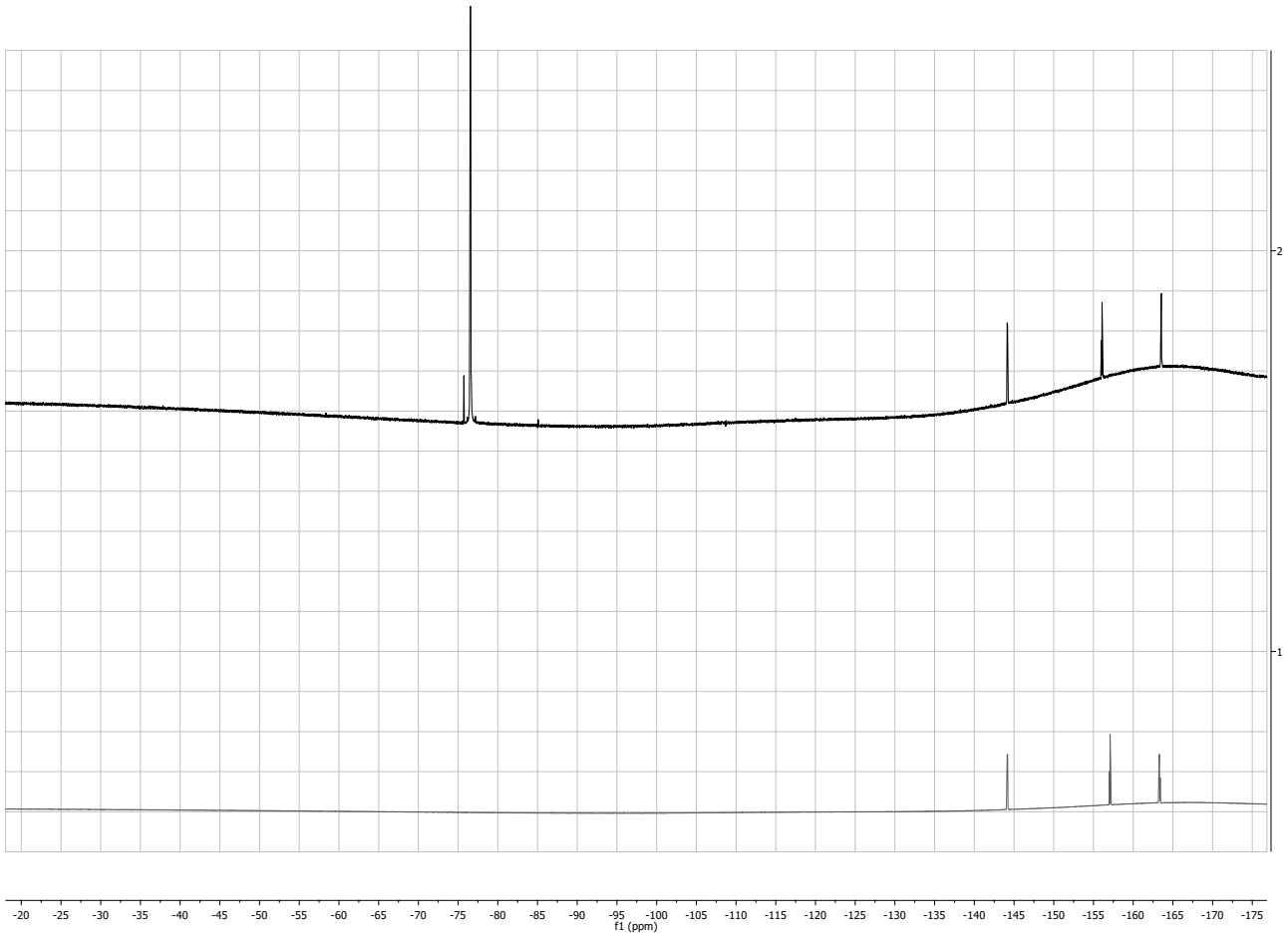

Fig. S 6 ^{19}F NMR of the FAP-d2 (black, with TFA-d_1 at -76.5 ppm) and FAP (dark grey) samples mentioned above.

UV/Vis optical data of ligands

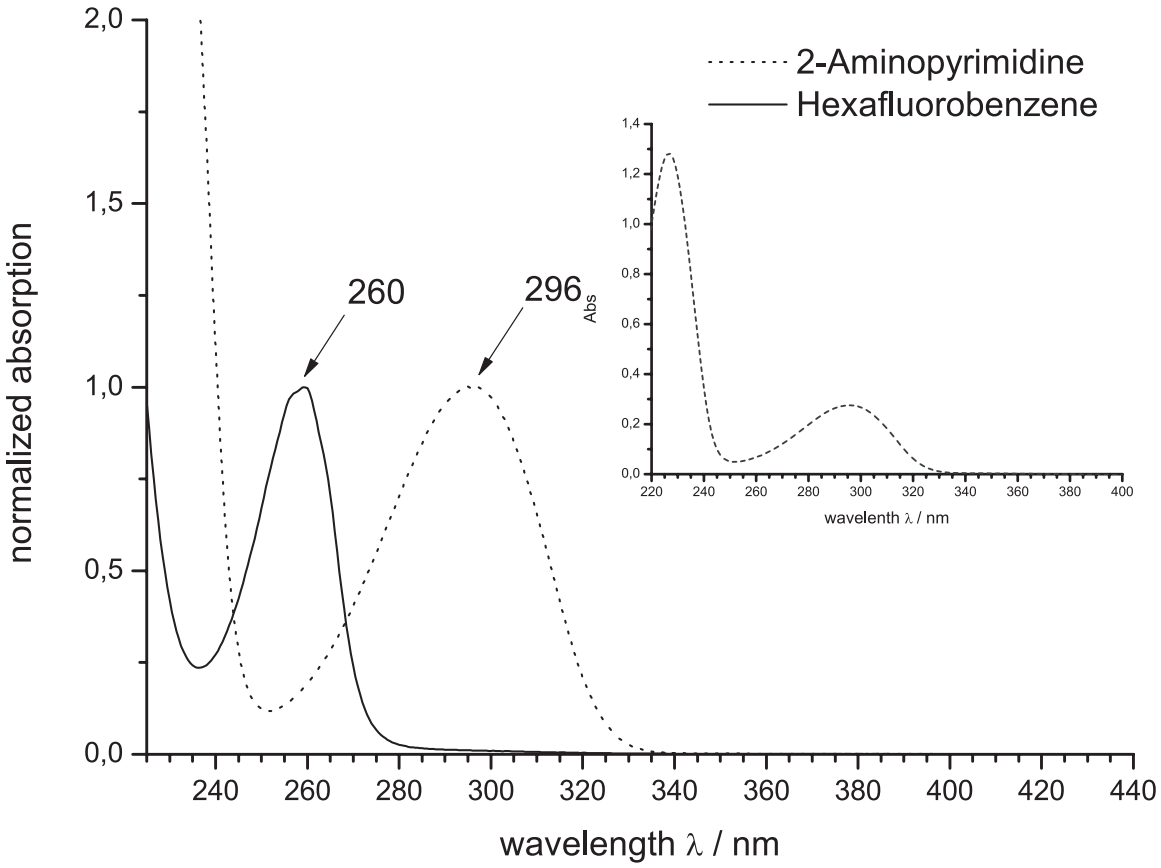

Fig. S 7 UV/Vis-absorption spectra (normalized) of 2-aminopyrimidine (dashed line, dark grey) and hexafluorobenzene (solid line, black) in EtOH. The inset shows the full spectra of 2-AP with UV-C region and the band maximum peaking at 227 nm.

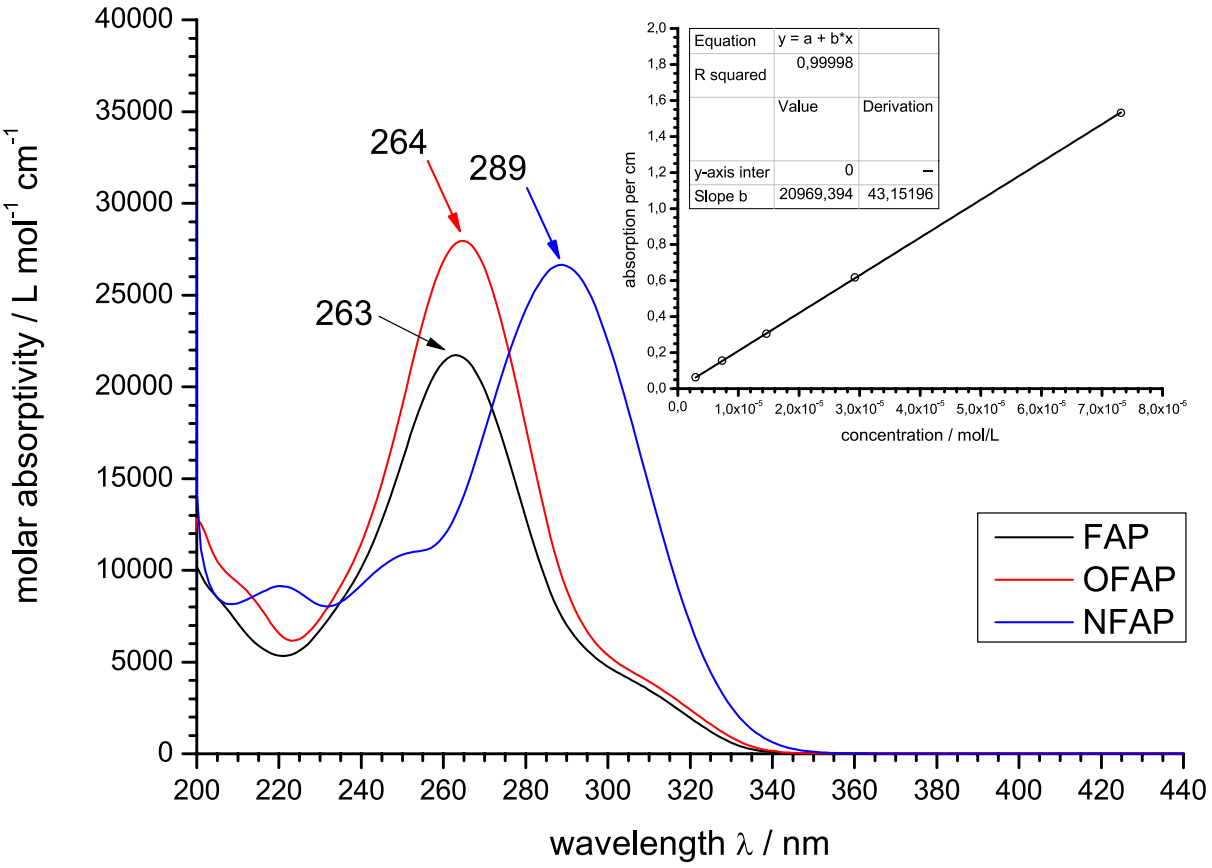

Fig. S 8 UV-Vis spectra as molar absorbivity of FAP, OFAP, NFAP in EtOH (black, red, blue). Inset shows a typical lambert-beer-fit for determination of ε (in this case for FAP). Each experiment was done two times independently. As the y-axis *a* intercept was usually in the range of the noise level of the instrument (0.001), fitting was done with parameter set to $a = 0$, which did not change the correlation coefficient. The given derivation in Table 2 is the mean error.

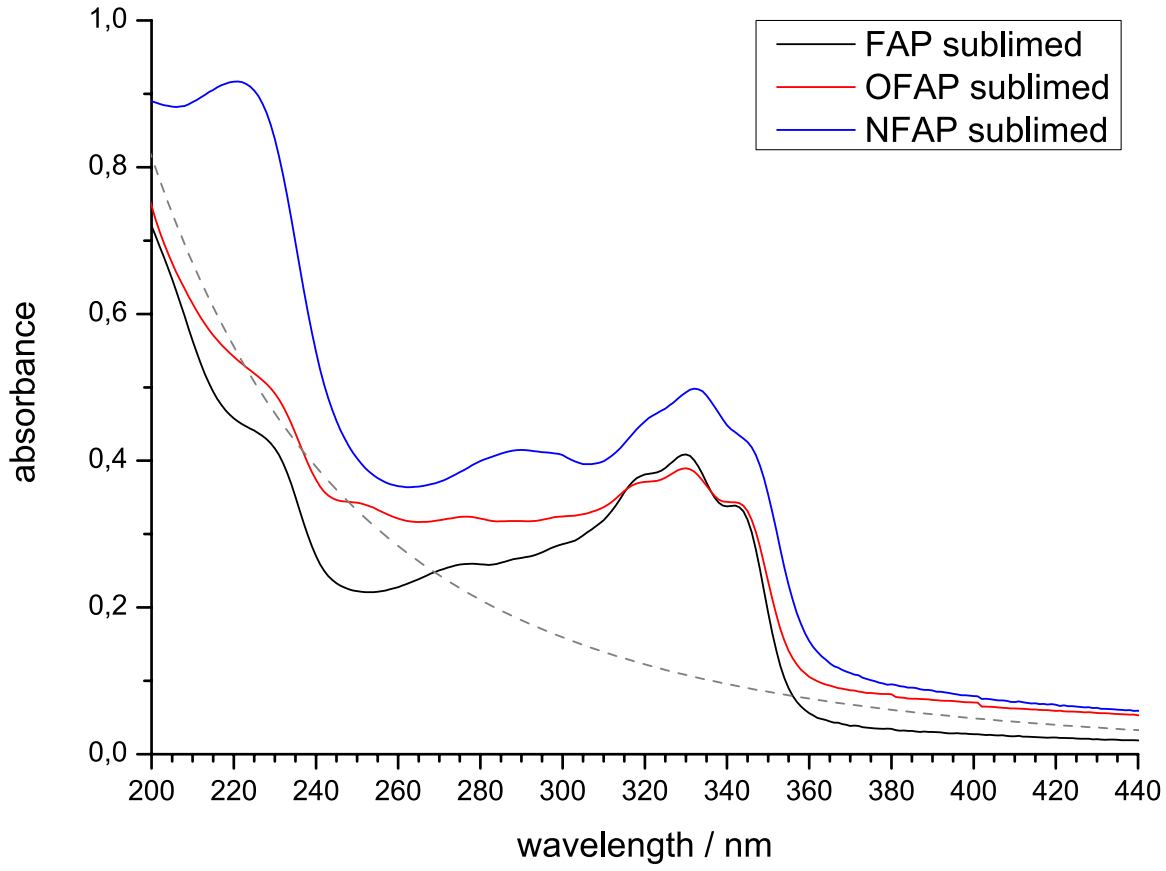

Fig. S 9 UV-Vis spectra of thin sublimed films of FAP, OFAP, NFAP (black, red, blue). The grey dashed line indicates the λ^4-dependent term of Rayleigh scattering (which is meant as guidance for the eye as exact particle/crystallite size distribution is unknown).

Infrared spectra of 2-AP and ligands 1 - 3

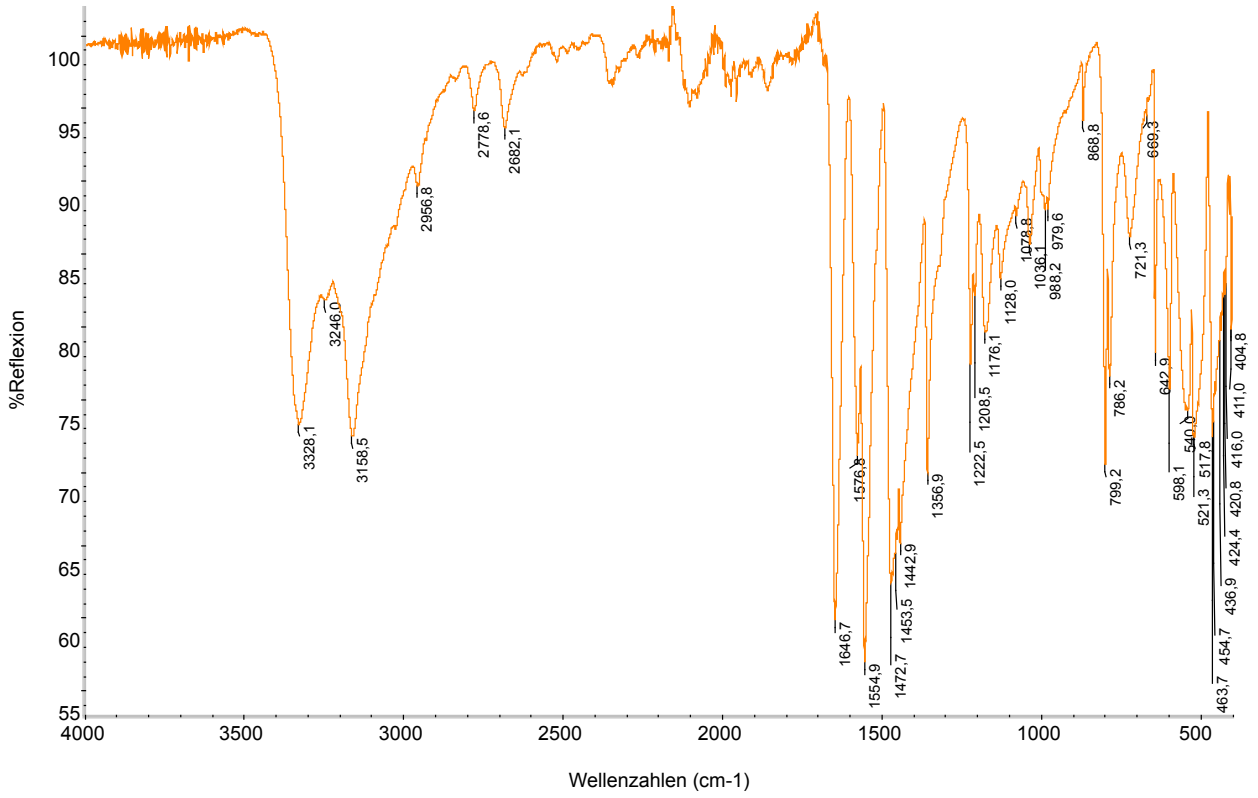

Fig. S 10 Infrared spectra (ATR) of 2-aminopyrimidine.

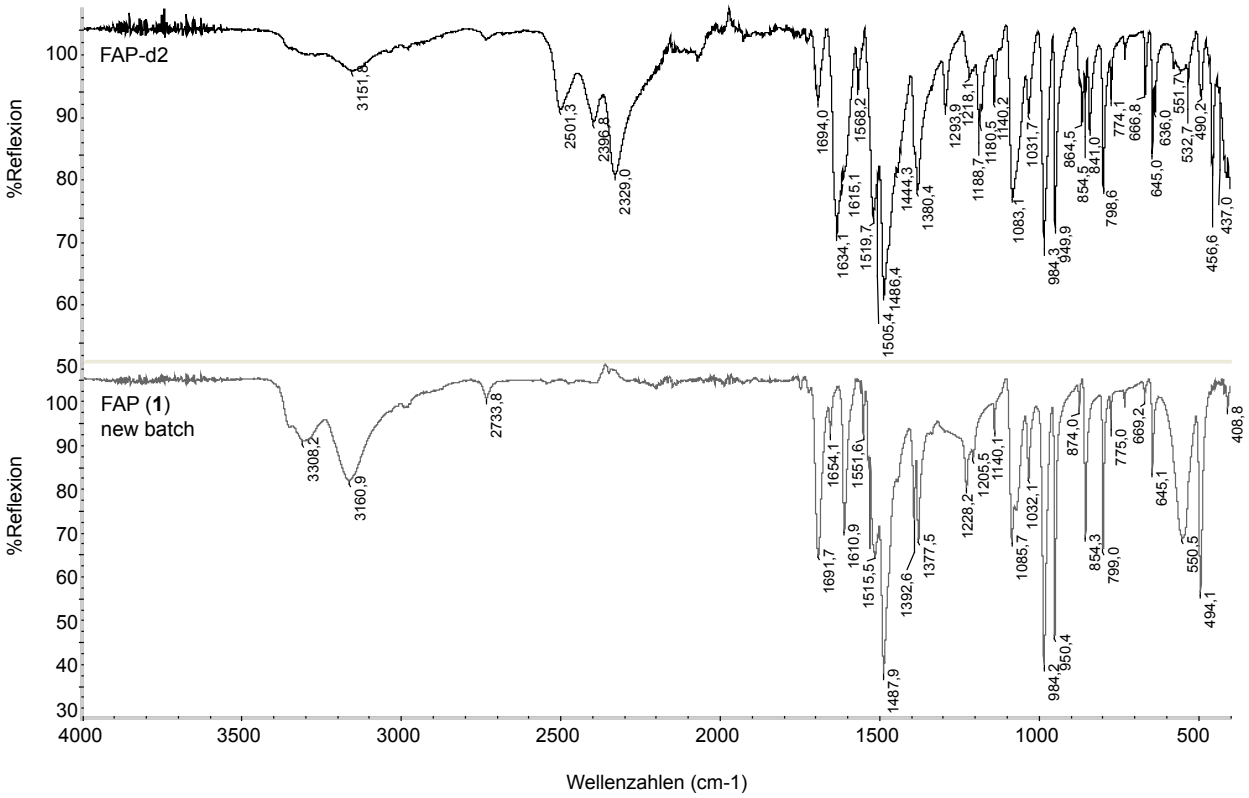

Fig. S 11 Infrared spectra (ATR) comparison of partially deuterated FAP-ND_2 (top, black) and **1** (bottom, grey).

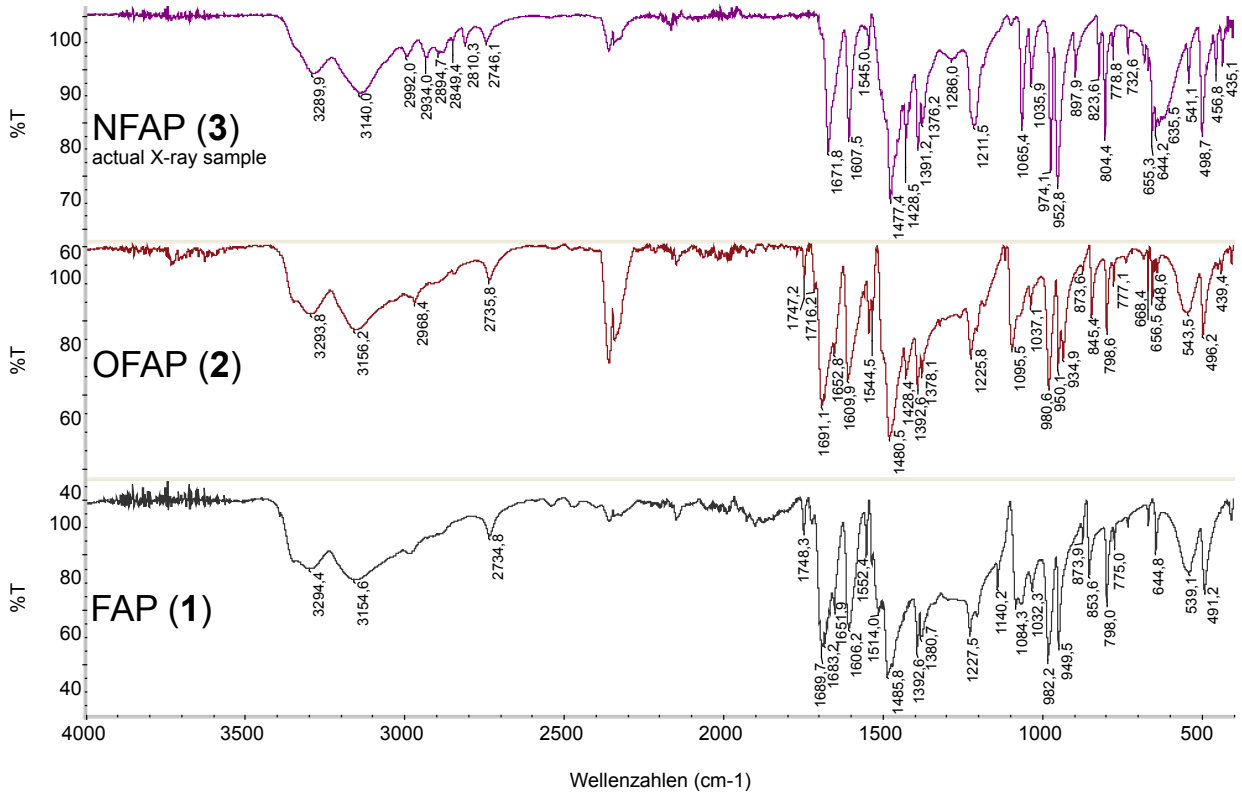

Fig. S 12 Infrared spectra (ATR) of compounds **1**, **2**, and **3**. Color coding as above (FAP shades of black, NFAP shades of blue, OFAP shades of red).

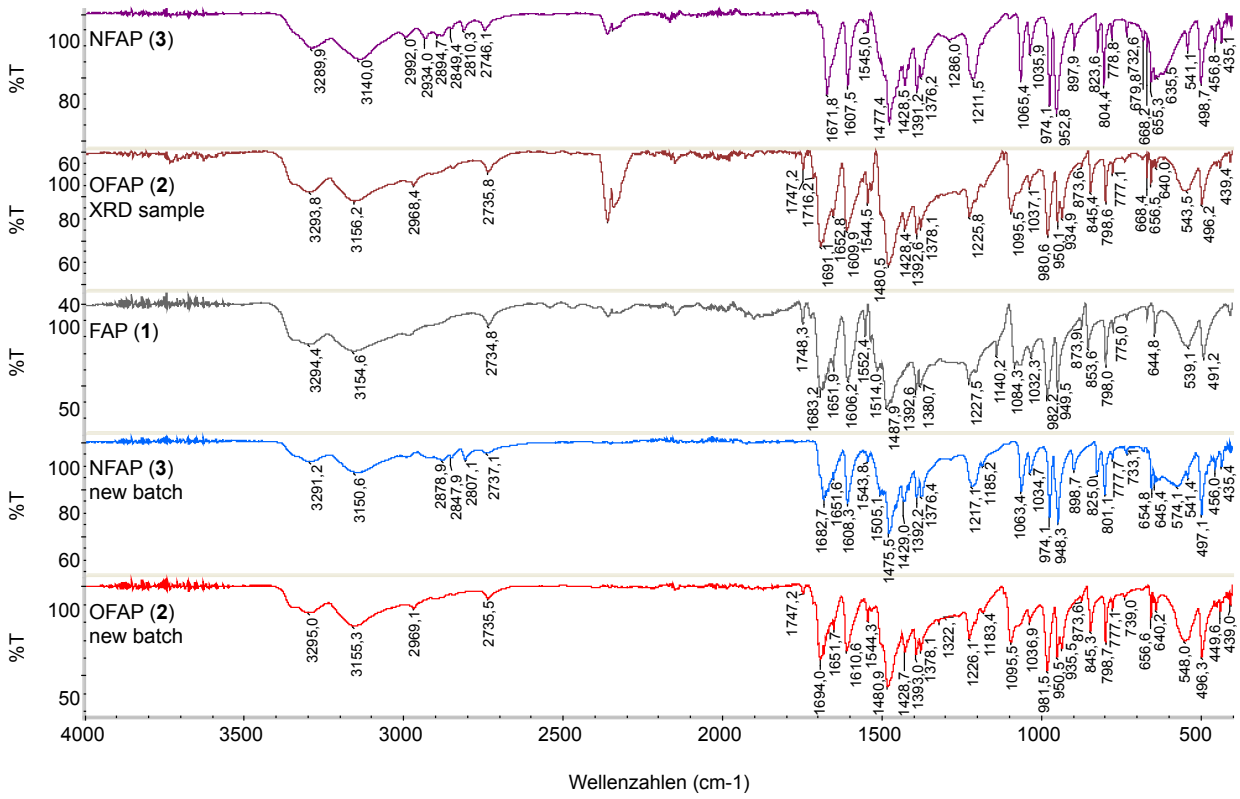

Fig. S 13 Comparison of infrared spectra between different batches of compounds **2** and **3**. IR spectra of **1** is given as reference. Color coding as before.

Computational chemistry for the ligands

The calculations were performed with the help of Gaussian 09 program.[19] The DFT B3LYP/6-31+G(d) method was used. All frequencies in harmonic approximation for the calculated minimum energy geometry were positive and are shown in Figure 16, Figure 17, and Figure 16 for FAP (**1**), OFAP (**2**), and NFAP (**3**) respectively.

FAP ligand

Calculated geometry formated as Z-matrix for the FAP ligand (**1**):

```
22

N          -3.38540         0.89900        -0.79920
N          -3.38490        -0.89460         0.80350
C          -3.99830        -0.00160        -0.00190
C          -2.05640        -0.88110         0.79070
H          -1.56720        -1.59740         1.44740
C          -1.30090         0.00120         0.00040
C          -2.05680         0.88680        -0.78580
H          -1.56800         1.60970        -1.43560
C           0.17780         0.00080         0.00010
C           0.92290        -1.18310        -0.11350
F           0.28990        -2.36450        -0.25060
C           2.31480        -1.19820        -0.11280
F           2.98110        -2.35530        -0.23330
C           3.01780        -0.00110        -0.00060
F           4.35610        -0.00200        -0.00090
C           2.31650         1.19690         0.11200
F           2.98440         2.35310         0.23250
C           0.92460         1.18360         0.11350
F           0.29330         2.36600         0.25150
N          -5.35640        -0.02480        -0.02750
H          -5.84720         0.71400        -0.50900
H          -5.84680        -0.58500         0.65380
```

OFAP ligand

Calculated geometry formated as Z-matrix for the OFAP ligand (**2**):

```
26

N          -3.69800        -0.96640        -0.74780
N          -5.67650        -0.11120         0.08600
H          -6.15000        -0.88230        -0.36130
H          -6.15730         0.40810         0.80580
N          -3.70820         0.81720         0.86400
C          -4.31530        -0.09160         0.07300
C          -2.38010         0.84810         0.81050
H          -1.89520         1.57740         1.45590
C          -1.61940        -0.00360        -0.00750
C          -2.37000        -0.90870        -0.77590
H          -1.87760        -1.61110        -1.44500
C          -0.14220         0.04490        -0.05080
C           0.65070        -1.10700         0.02790
F           0.06590        -2.31740         0.15760
C           2.04110        -1.07280        -0.01990
F           2.71850        -2.24180         0.02670
C           2.73660         0.13990        -0.12100
C           1.95570         1.30410        -0.20040
F           2.56560         2.49610        -0.31210
C           0.56820         1.24940        -0.17220
F          -0.10470         2.41490        -0.27190
C           4.93230        -0.54620         0.60440
H           4.53930        -0.61520         1.62450
H           5.89500        -0.03290         0.61310
H           5.04370        -1.54530         0.17690
O           4.07860         0.27750        -0.21200
```

NFAP ligand

Calculated geometry formated as Z-matrix for the NFAP ligand (**3**):

```
30

N          3.96880       -0.90560        0.83510
N          5.96020       -0.01470        0.06970
H          6.42970       -0.77680        0.53670
H          6.45430        0.49190       -0.65040
N          4.00300        0.84930       -0.80650
C          4.59820       -0.03020        0.02490
C          2.67310        0.84980       -0.80670
H          2.19840        1.55500       -1.48540
C          1.89900       -0.00400       -0.00320
C          2.63930       -0.87860        0.80960
H          2.13720       -1.58160        1.47040
C          0.42120        0.01280       -0.01760
C         -0.34970       -1.15390       -0.08660
F          0.26200       -2.35790       -0.14400
C         -1.74080       -1.14450       -0.07980
F         -2.37300       -2.34150       -0.08670
C         -2.48740        0.04870       -0.05320
N         -3.88030        0.12740       -0.11790
C         -1.70860        1.22390        0.00640
F         -2.32610        2.42510        0.01690
C         -0.32240        1.20190        0.03900
F          0.32010        2.38830        0.11400
C         -4.64070       -0.91620       -0.79840
C         -4.58710        0.74060        1.00740
H         -4.09870       -1.26170       -1.68130
H         -5.58910       -0.47840       -1.13090
H         -4.86340       -1.78330       -0.15870
H         -4.02780        1.59220        1.39610
H         -4.75300        0.01990        1.82610
H         -5.56140        1.10200        0.66130
```

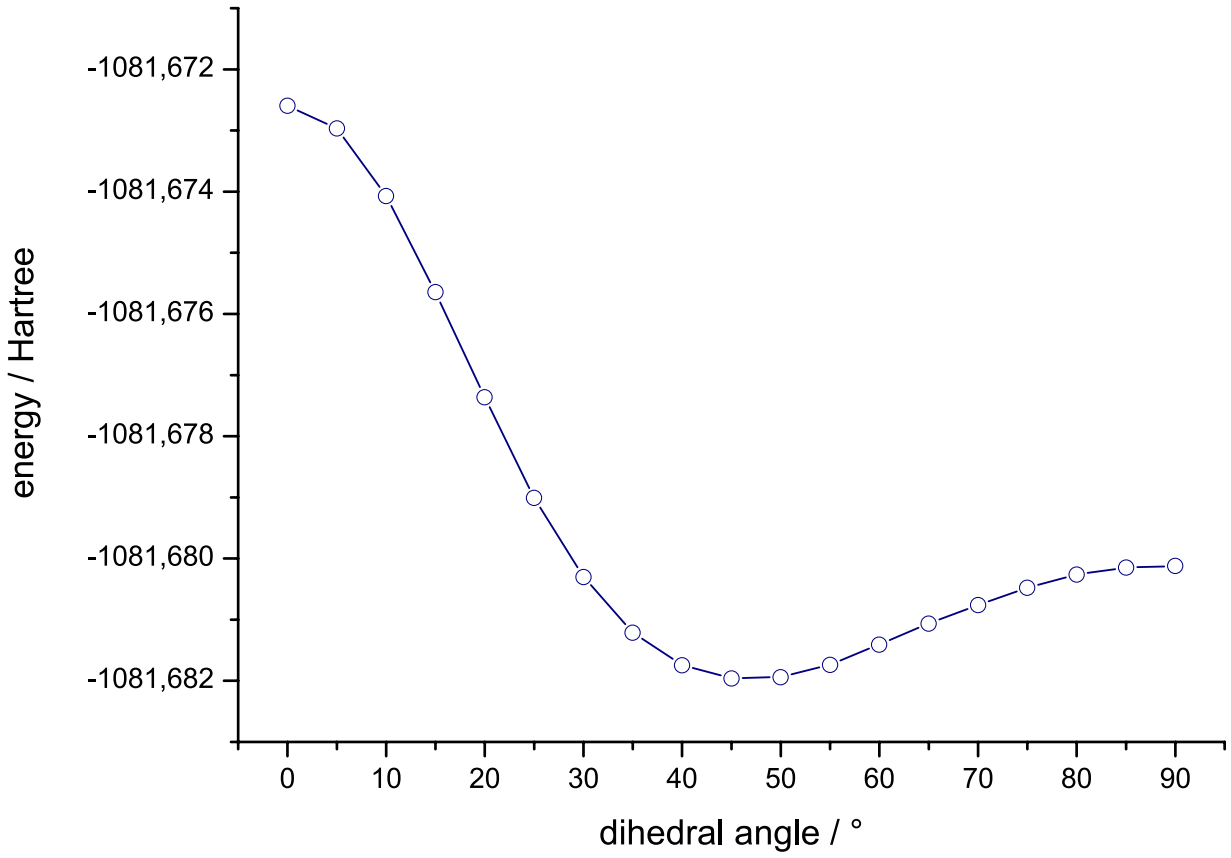

Fig. S 14 Calculated single point energies (B3LYP 6-31+G(d)) for optimized structures of the NFAP ligand with manually set dihedral twist angles ϕ.

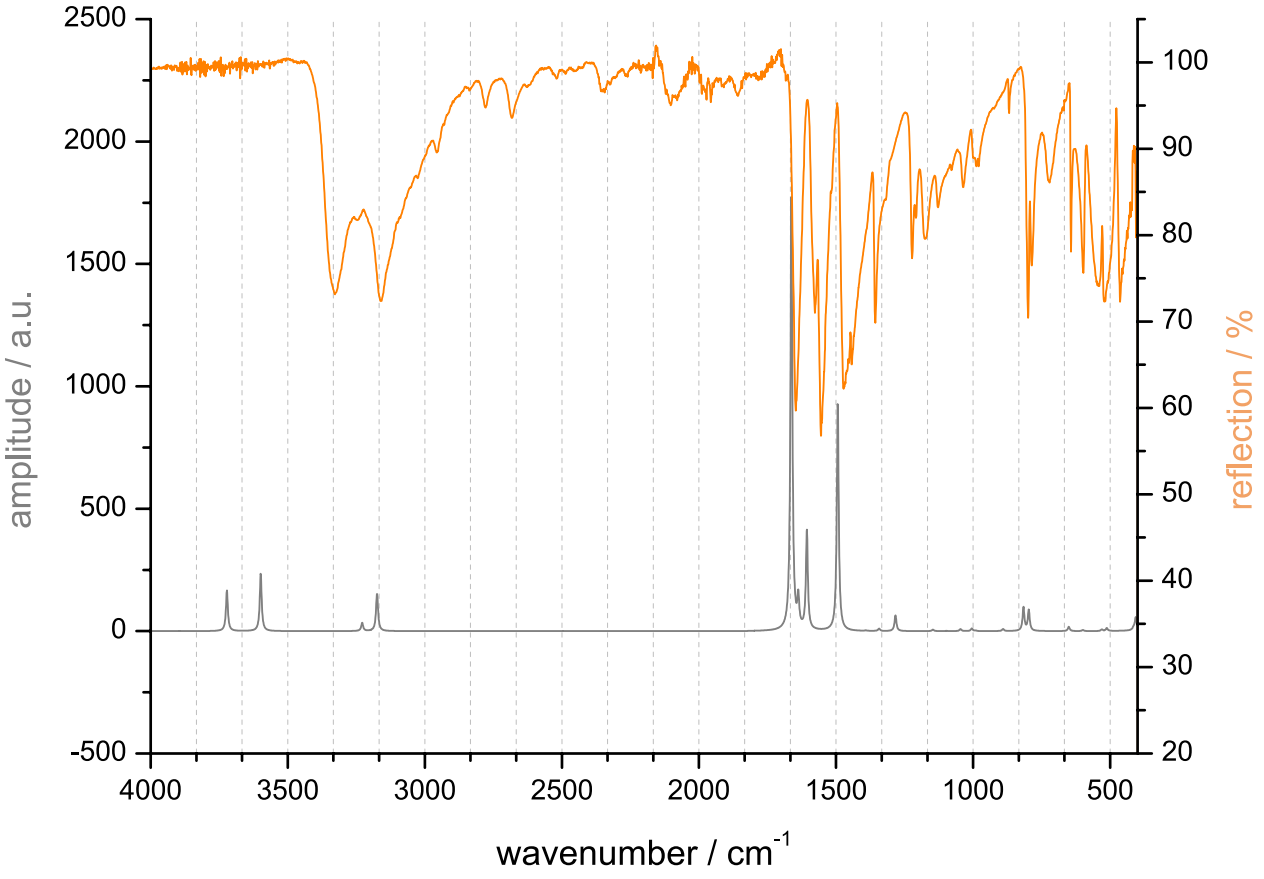

Fig. S 15 Comparison of infrared spectra of 2-AP (orange colored) and simulated gas-phase spectra from DFT calculations on B3LYP/6-31+G(d) level (grey).

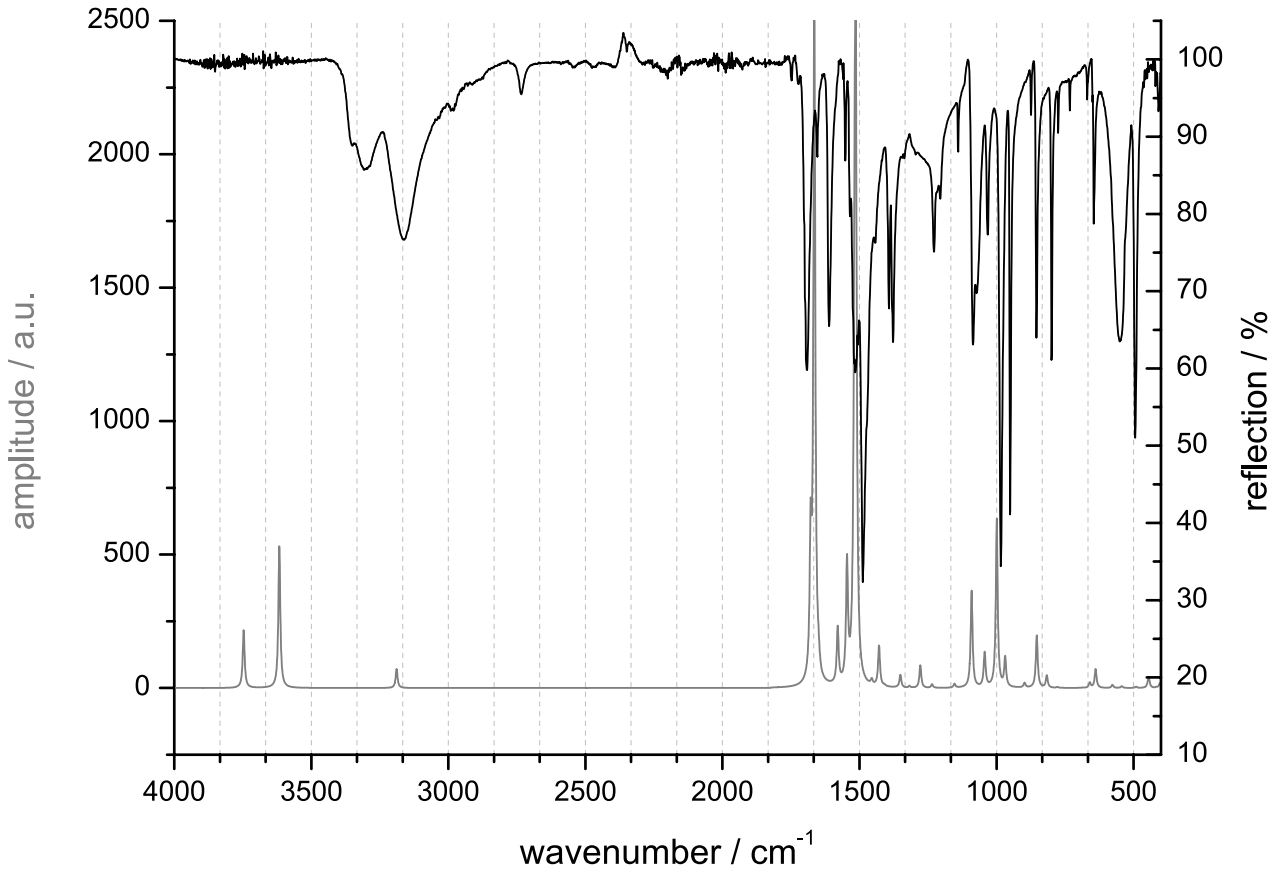

Fig. S 16 Comparison of infrared spectra of ligand **1** (black) and simulated gas-phase spectra from DFT calculations on B3LYP/6-31+G(d) level (grey).

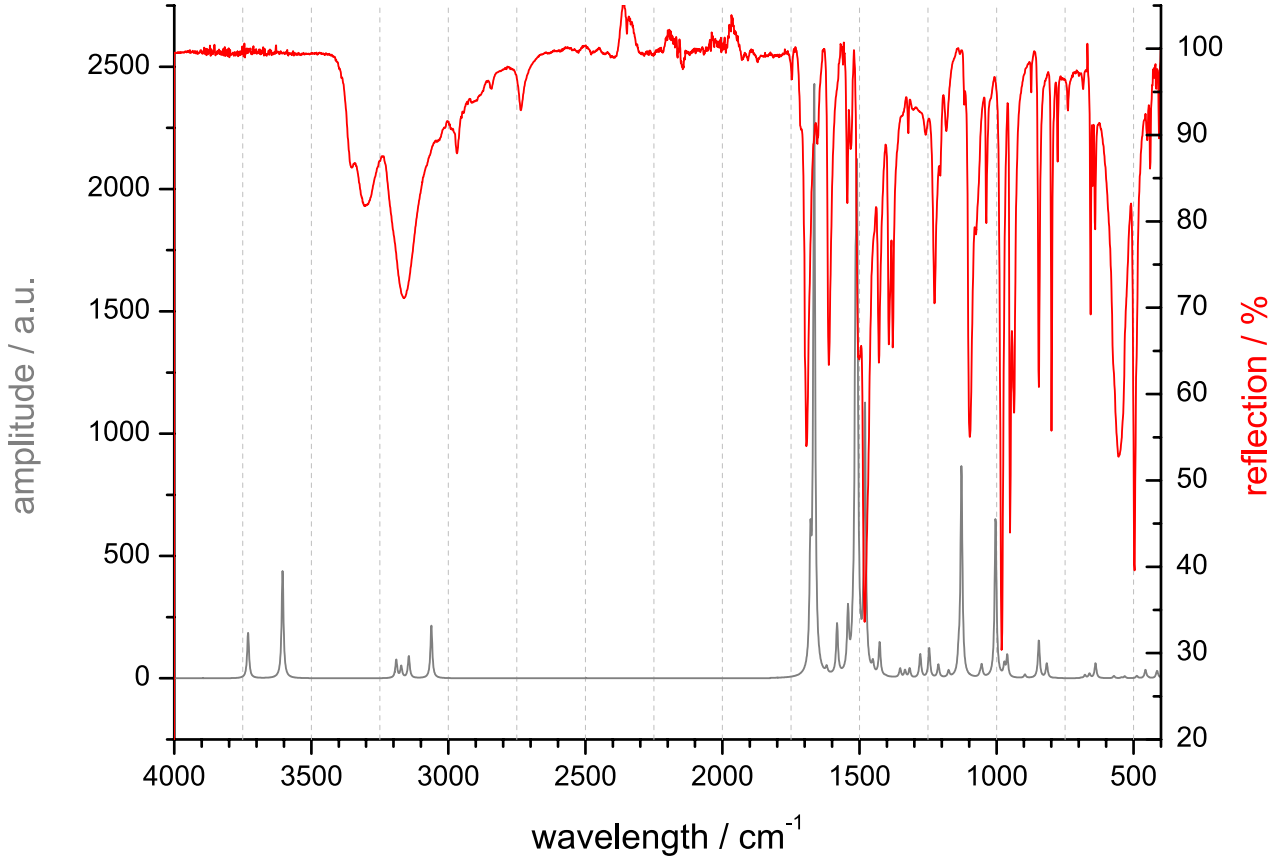

Fig. S 17 Comparison of infrared spectra of ligand **2** (red) and simulated gas-phase spectra from DFT calculations on B3LYP/6-31+G(d) level (grey).

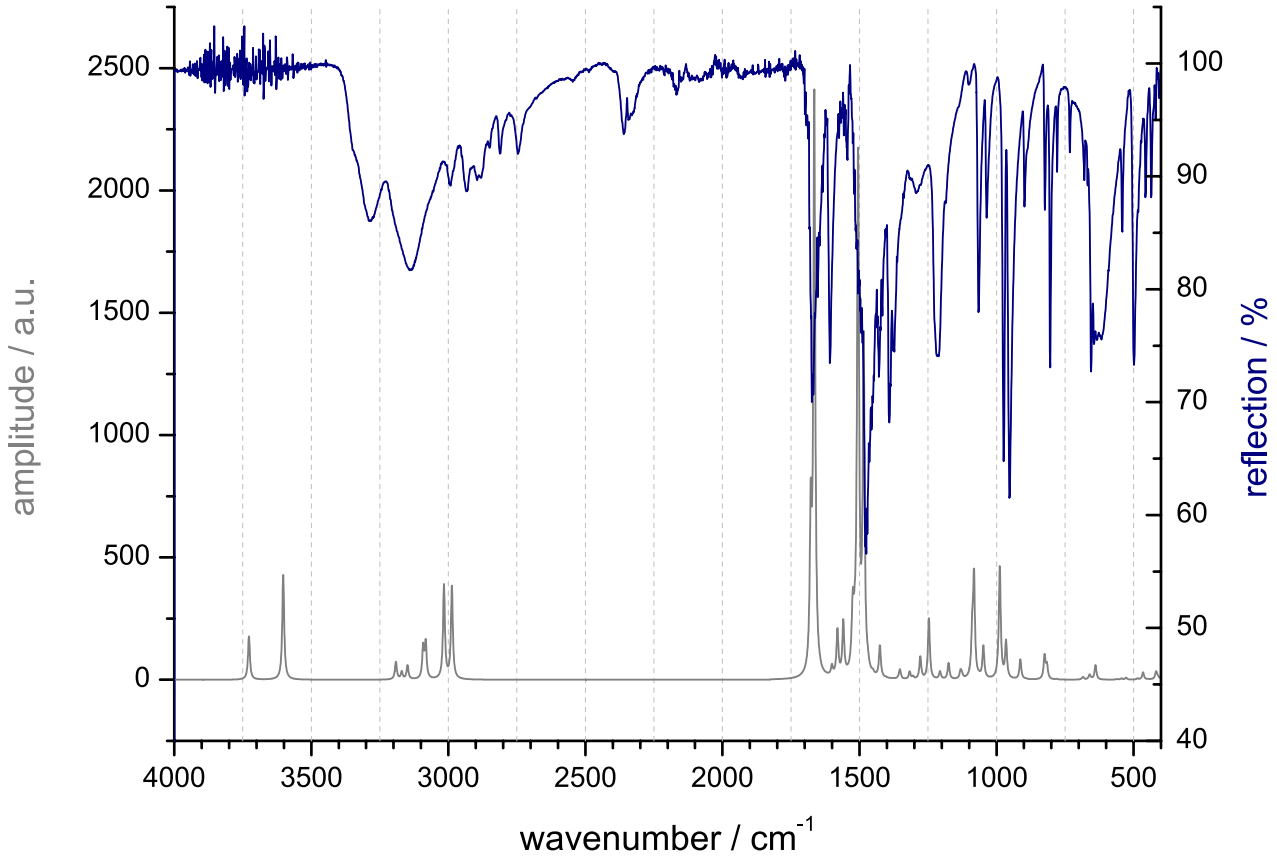

Fig. S 18 Comparison of infrared spectra of ligand **3** (blue) and simulated gas-phase spectra from DFT calculations on B3LYP/6-31+G(d) level (grey).

Infrared spectroscopy of the coordination compounds

IR spectra of Smith crystals and CPs 4 - 11b

As mentioned in the IR section of the ligands some detailed infrared studies on metal ion complexes of 2-AP are reported. In detail, 2-AP complexes of Zn^{II}, Cd^{II} and Hg^{II} halide complexes are reported by Contreras *et al.*,[4] while Mn^{II}, Co^{II}, Ni^{II} and Cd^{II} in 2D coordination compounds bridged by $Ni(CN)_4^{2-}$ were investigated by Akyuz,[5] and finally some studies on Sn^{II} and Sn^{IV} halides were published by Kovala-Demertzi *et al.*[6] It is reported by them that "the ring modes are very little affected by coordination, whereas the N−H stretching modes are shifted by 50-200 cm^{-1}."[4] The higher frequency shift indicate that the amino group "does not take part in coordination."[5–7]

The very same behavior is visible for the *catena*-coordination compounds reported here. We found similar high frequencies shifts implying a less pronounced hydrogen bonding in comparison to 2-AP in the solid-state as pointed out by several authors.[4–6] Often a splitting of N−H stretch bands into three or four narrower bands was found (exception are TFA compounds **4** and **8**) indicating the the presence of free and associated N−H groups.[6] This splitting was also shown but not interpreted by Contreras *et al.* for the Hg^{II} and Zn^{II} halide complexes.[4] In fact, aside from this feature, it is hardly possible to distinguish coordination compounds from free ligand on first glance as most bands of the ligands are conserved in the CPs (e.g. 1608, 1220, 1066, 1045, 980, 949, and the 799, 777 cm^{-1} couple; all ± 6 cm^{-1}). The strong and broad band at 1480 cm^{-1} is also conserved but the intensity is lower for the NFAP CP series **8** - **11b**.

In summary, only the anion of the used Ag^{I} salt gives rise to new bands. Nevertheless one clear feature is visible in all spectra of the FAP series CPs **4** - **11b**: The formerly broad feature at about 1690 cm^{-1} narrows and shifts to lower energy (1648 to 1630 cm^{-1}). Only the TFA compounds **4** and **8** show still a feature rich broad absorption band which can be ascribed by additional visible anion bands (*vide supra*). Compounds **7** and **10** express an even more pronounced shift of the 1690-band. Furthermore the weak, unassigned 2735 cm^{-1} band disappears for the coordination compounds **4** - **11b**.

The report of Akyuz comprises coordination sensitive bands of the 2-AP ring modes. This can be compared to our results of the FAP series CPs **4** - **11b** and moreover $[Ag(ap)(pts)]_n$, which was not detailed studied in terms of IR spectroscopy by Smith *et al.*[8] For the latter mentioned – and most comparable case – indeed similar shift are visible as reported by Akyuz.[5] The band of the 2-AP ring stretch at 1577 cm^{-1} moves to 1588 cm^{-1} as and similar the 1555 cm^{-1} absorption to 1568 cm^{-1}. Other band shifts (e.g. 1444 to 1460 cm^{-1}) are hard to follow as they appear as weak shoulders of the strong 1472 cm^{-1} band and are therefore difficult to observe. The 1176 cm^{-1} band remains unchanged in this case and the (possible shift of the) weak 1078 cm^{-1} mode is not visible anymore in the CP (probably covered by the broad 1106 cm^{-1} band of *p*-toluenesulfonate)[9] None of these marker bands can be followed in case of the FAP series CPs **4** - **11b**.

TFA^- CPs:

In case of Ag^{I}TFA compounds **4** and **8** (Figure S 20 and S 24) the low frequency N−H stretching absorption at 3150 cm^1 is not preserved but shifted close to 3190 ± 8 cm^{-1}. The high frequency N−H band is shifted to 3322 ± 5 cm^{-1} but still close to the 3300 ± 10 cm^{-1} value found for the ligands. The expected strong bands of the symmetric and asym. COO vibration in the lower wavenumber region (1660, 1450 cm^{-1}) are visible at 1663 cm^{-1} for both compounds thorough the induced shift of the former broad 1690 cm^{-1} ligand mode to about 1644 cm^{-1}, while the lower wavenumber TFA mode remains indistinguishable from ligand bands in this region. However, strong bands at 1187 ± 2 cm^{-1} and 1137 ± 2 cm^{-1} are apparent which can be clearly assigned to C−F stretch modes of the TFA anion.[10] The medium strong bands expected for TFA at around 845 cm^{-1} (C−C stretch) and at 800 cm^{-1} (assignment ambiguous) are at ligands band positions. Only for NFAP where the 845-mode is located at 825 cm^{-1} the second band at 837 cm^{-1} can be assigned to the C−C stretching vibration. Another good probe mode can be found at about 722 cm^{-1} for both compounds, which matches the reported value for TFA perfectly, but has different assignments in the literature.[10] Other expected TFA bands (600, 515, 453 cm^{-1}; all ± 8 cm^{-1}) fall into a broad and feature rich region but appropriate shoulders are visible (**4**: 518, 454 cm^{-1}; **8**: 520, 459 cm^{-1})

OTf^- CPs:

The triflate CPs **5** and **9** (Figure 21 and 25) include one molecule ethanol per repetition unit, which is not distinctive in IR spectra. The high frequency bands at 3400 cm^{-1}, 3330 cm^{-1}, and 3230 cm^{-1} can be assigned to the AP part. The latter two correlate well with the shift observed for the other CPs of **2** and **3**. The high energy band is the second highest observed in this series only exceeded by the ClO_4^- coordination polymers **6** and **10**. As pointed out above it is a indicates for unassociated N−H stretching

vibration and indeed the crystal structure show only hydrogen-bonding to one side of the amino group along the helical structure of **5** and **9**. The broad peak with shoulders at about 1250 to 1210 cm^{-1} (including the 1220 cm^{-1} ligand band) is probably of the OTf anion, although these are 20 - 10 cm^{-1} lower then reported.[11] Good matching was found for the 1165 cm^{-1} band and the intense 638 cm^{-1} band. Another OTf related band might be located at the intense 1026 cm^{-1} transition, not observed otherwise, but which is again 15 - 5 cm^{-1} lower then reported.[11]

ClO_4^- CPs:

Both perchlorate CPs **6** and **10** (Figure S 21 and S 26) show a distinctive, congruent three bands pattern in the IR high energy region. Bands are located at 3450, 3357, and 3234 cm^{-1}. These positions match a description for 2-aminopyridine perchlorate compounds by Beauchamp *et al.*[7] well, but here, for 2-AP-based compounds, an additional high energy shift of approx. 10 cm^{-1} is found. From the crystal structure of **6** and **10** it can be deduced that only one side of the amino group of 2-AP participates in hydrogen-bonding along the polymer axis, which would, similar to **5** and **9**, explain the highest energy band.

The strong absorptions of the perchlorate ion are visible at 1107 cm^{-1} (ν_3) and 617 cm^{-1} (ν_4) for **6**. The ν_1-mode of perchlorate is difficult to assign as several bands are visible in this region. On comparison with the ligand spectra and other CPs the weak 909 cm^{-1} band is the most reasonable one. Interestingly the difference in structure of CP **6** (network) and **10** (μ-bridged κ(O,O') double strand) is reflected in the IR spectra, as for **10** the ν_3-mode is found at 1049 cm^{-1} (very broad). This value matches the description of bridged $M^+ClO_4^-$ dimers and also of a trinuclear 2-aminopyridine silver perchlorate complex.[7,12] A splitted band peaking at 1147 and 1136 cm^{-1} is also found but it is not clear if this belongs to the (usual broad) perchlorate ν_3 triplet. The ν_4-mode of **10** can be found at 618 cm^{-1} with a shoulder at 628 cm^{-1} while the weak 919 cm^{-1} band is probably the ν_1 mode of perchlorate. Both match the literature values well.[12–15]

NO_3^- CPs:

The CPs assembled of silver nitrate and FAP series ligands, among them the polymorph **11a** and **11b** (Figure S 26, S 27 and S 28), show only partial congruent bands for the N−H modes. The highest energy mode is found at 3397 cm^{-1} for **7**, while a weaker band is found at 3382 cm^{-1} for **11a**, only a shoulder is found at 3361 cm^{-1} for **11b**. An intense band is found at 3300 cm^{-1} for **7** and **11b** but at 3325 cm^{-1} for **11a**. A similar shift is found for the second band in the lower energy region at 3211 cm^{-1} for **7**, 3204 cm^{-1} for **11b** but 3225 cm^{-1} for **11a**. CP **11a** shows also a weak band at 3268 cm^{-1}, a value otherwise only observed for **5**. The differences probably reflect the different environments for the AP head found in the crystal structures of **7**, **11a**, and **11b**.

The NO_3^- CPs show a broad and variable strong band in the 1400 to 1300 cm^{-1} region which is typical for the nitrate ν_3 mode. As pointed out above bands at about 1392 and 1377 cm^{-1} (if visible) belong to the ligand, which let us conclude to assign the dominating 1299 cm^{-1} (with high energy shoulder) to the nitrate ion absorption for **7**. For **11a** and **11b** the assignment is difficult: for **11a** the (probably degenerated) broad bands at 1364 and 1318 cm^{-1} (with low energy shoulder) belong to the nitrate ion. For polymorph**11b** only a medium intense band at 1277 cm^{-1} is left for assignment in this region as the next bands (approx. 1220 and 1205 cm^{-1}) belong to the ligand. This transition might serve as indication for **11b**. It is noteworthy in this context that **7**, **11a** and **11b** show also a different pronunciation of the above mentioned 1690-band-shift to lower energy.

All CPs posses a band at about 820 cm^{-1}. For the NFAP based CPs **11a** and **11b** this interferes with a ligand band of **3** (825 cm^{-1}), while for **7** the ligand band (845 cm^{-1}) is found at 841 cm^{-1} and the 820 cm^{-1} band can therefore be assigned exclusively to the ν_2 mode of the nitrate ion.[13,16,17] Similar values where found by Beauchamp *et al.*[7] A conclusion of the binding mode of the NO_3^- ion by overtone analysis is not possible.[18] Only for **7** a very weak overtone (unindexed) appears at 1758 cm^{-1}, which is unfortunately a region where several binding modes overtones appear.

$[Ag(ap)SO_3C_6H_4CH_3]_n$ (Smith crystals):

IR (ATR): $\tilde{\nu}$ = 3372, 3317, 3240, 3209, 1652, 1588, 1568, 1505, 1368, 1212, 1157, 1119, 1106, 1028, 1006, 976, 855, 820, 790, 781, 685, 660, 560, 515, 468 cm^{-1}.

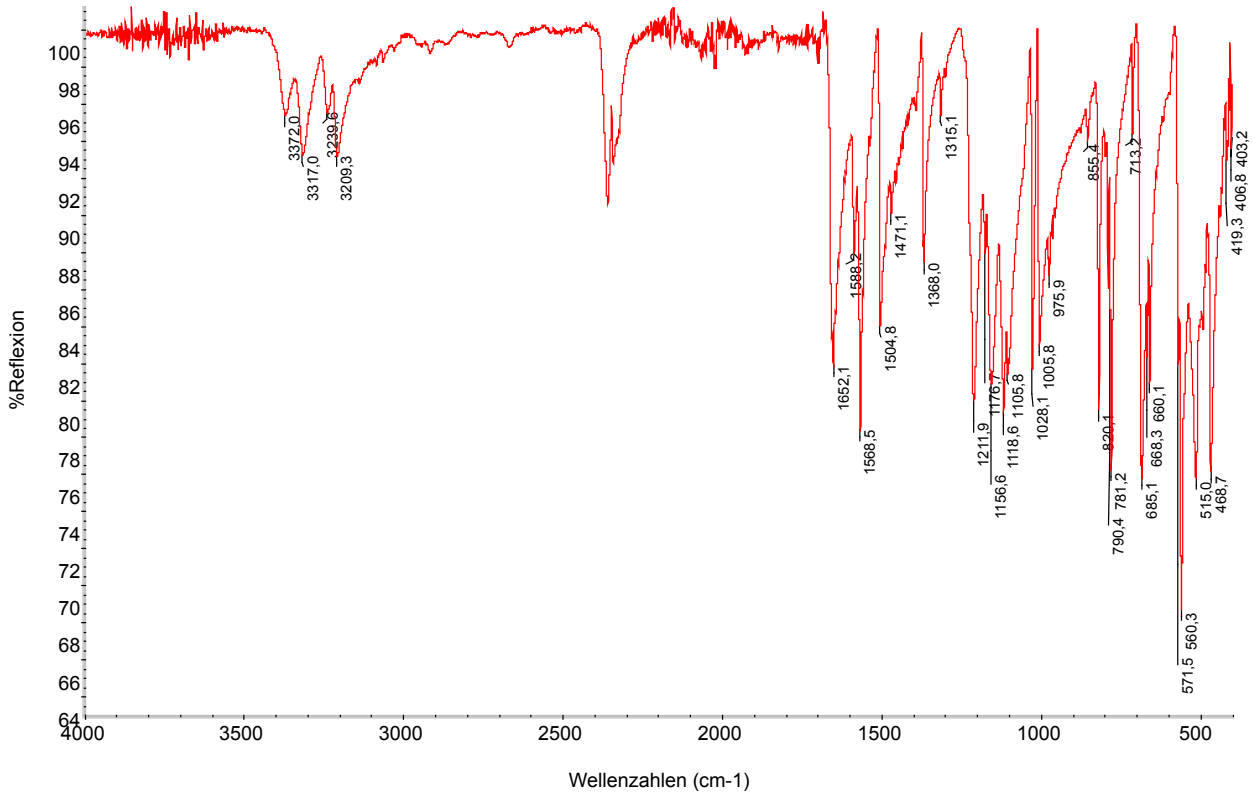

Fig. S 19 Infrared spectra (ATR) of Smith's crystals.

$[Ag(ofap)CO_2CF_3]_n$ (4):

IR (ATR): $\tilde{\nu}$ = 3368, 3317, 3199, 3019, 2964, 2844, 1655, 1637, 1608, 1490, 1427, 1387, 1370, 1221, 1186, 1135, 1097, 986, 946, 847, 793, 778, 721, 518, 486 cm^{-1}.

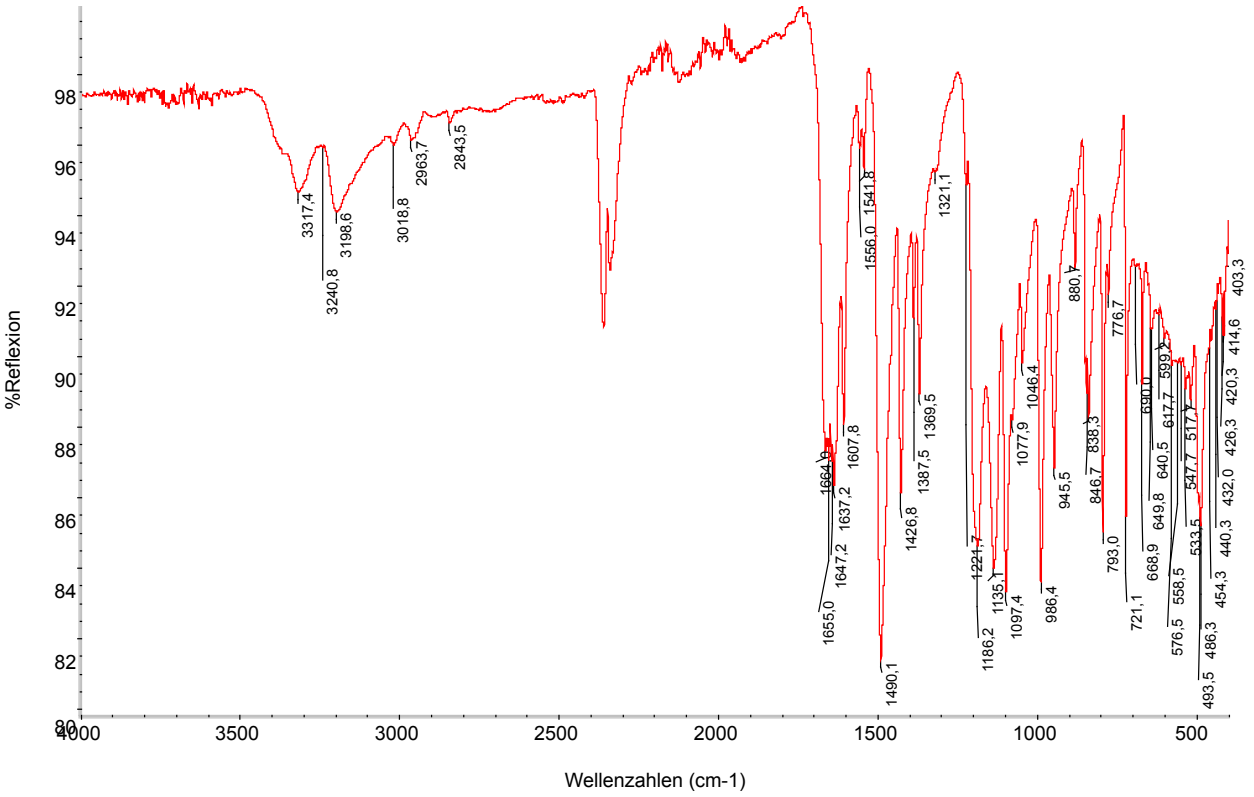

Fig. S 20 Infrared spectra (ATR) of compound **4**.

$[Ag(ofap)SO_3CF_3 \cdot EtOH]_n$ (5):

IR (ATR): $\tilde{\nu}$ = 3407, 3327, 3268, 3231, 3077, 2980, 2901, 1644, 1611, 1488, 1426, 1377, 1243, 1224, 1165, 1100, 1074, 1027, 986, 950, 874, 846, 796, 669, 638, 563, 492, 440 cm^{-1}.

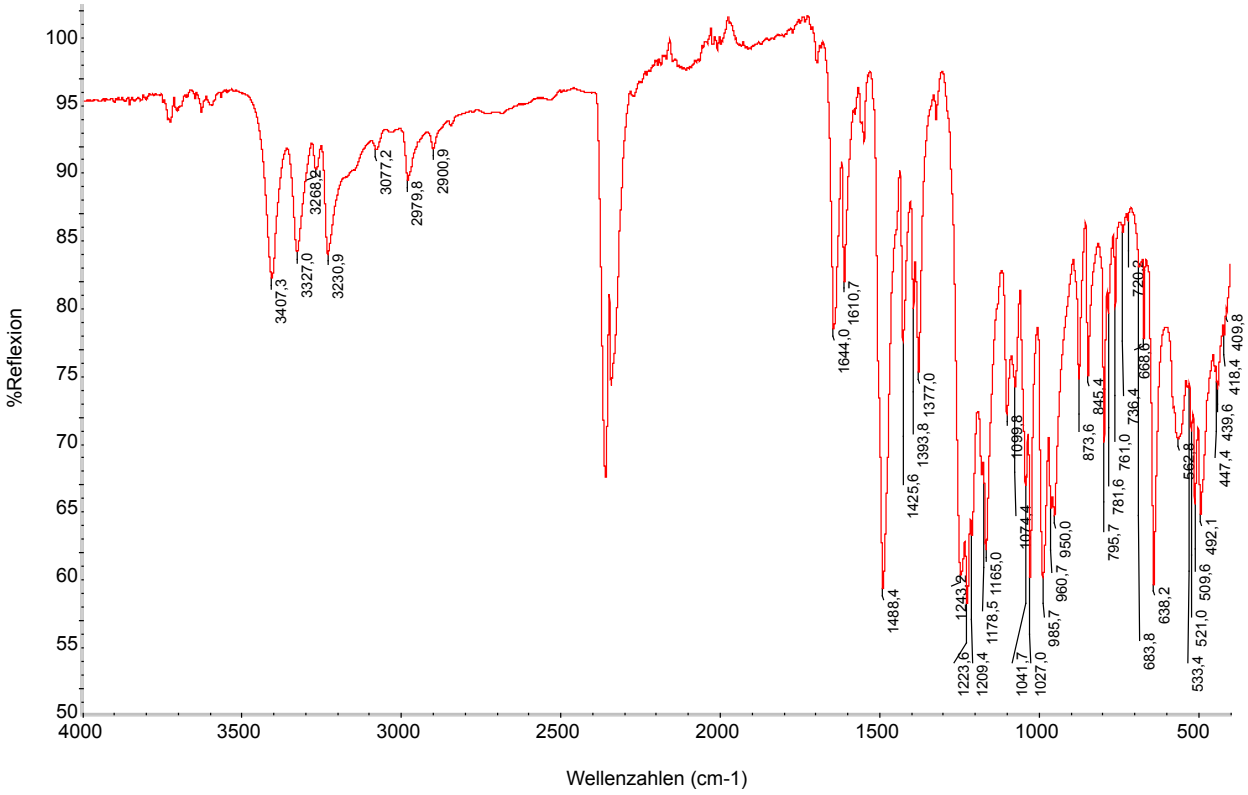

Fig. S 21 Infrared spectra (ATR) of compound **5**.

$[Ag(ofap)ClO_4]_n$ (6):

IR (ATR): = 3448, 3357, 3236, 3026, 2968, 2835, 1645, 1610, 1552, 1488, 1425, 1386, 1371, 1222, 1187, 1140, 1107, 991, 940, 910, 846, 796, 617, 536, 481 cm^{-1}.

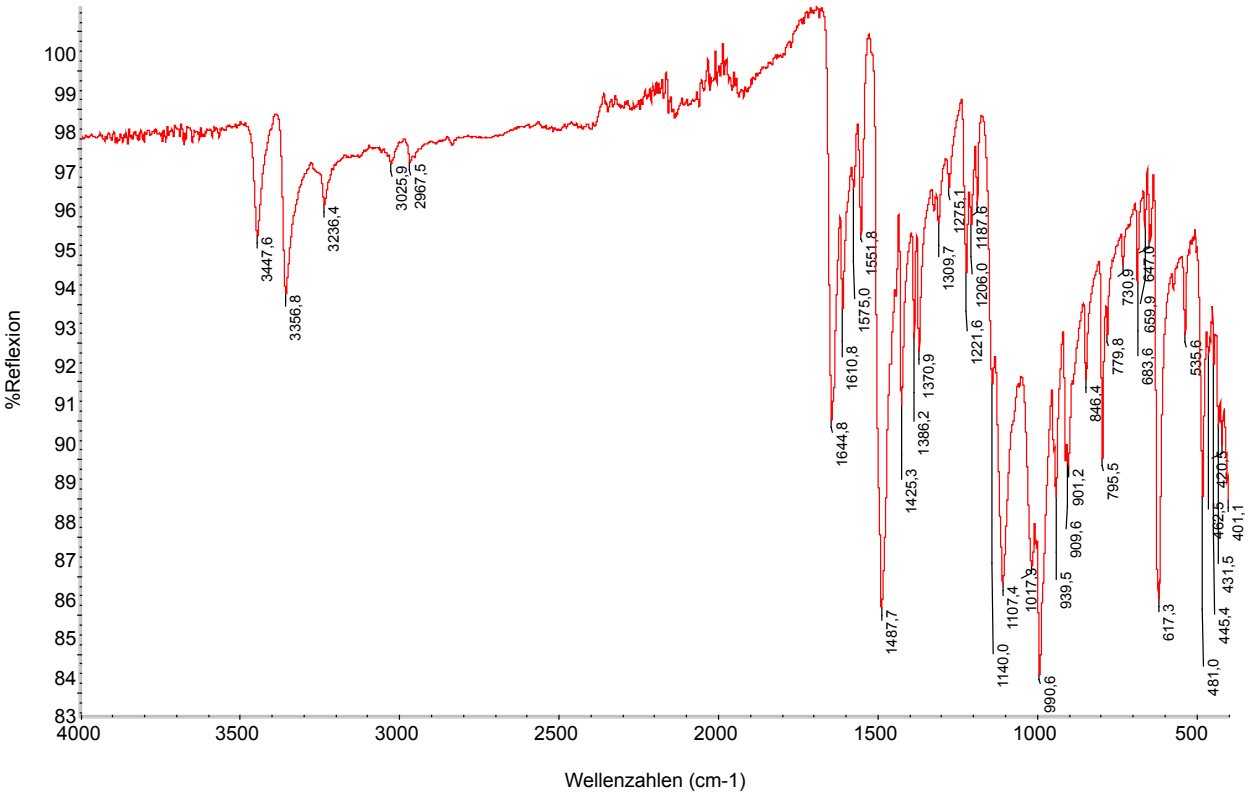

Fig. S 22 Infrared spectra (ATR) of compound **6**.

$[Ag(ofap)NO_3]]_n$ (7):

IR (ATR): $\tilde{\nu}$ = 3397, 3303, 3211, 2945, 2841, 1629, 1602, 1483, 1424, 1387, 1377, 1300, 1220, 1096, 1042, 978, 948, 841, 819, 797, 666, 560, 530, 471 cm^{-1}.

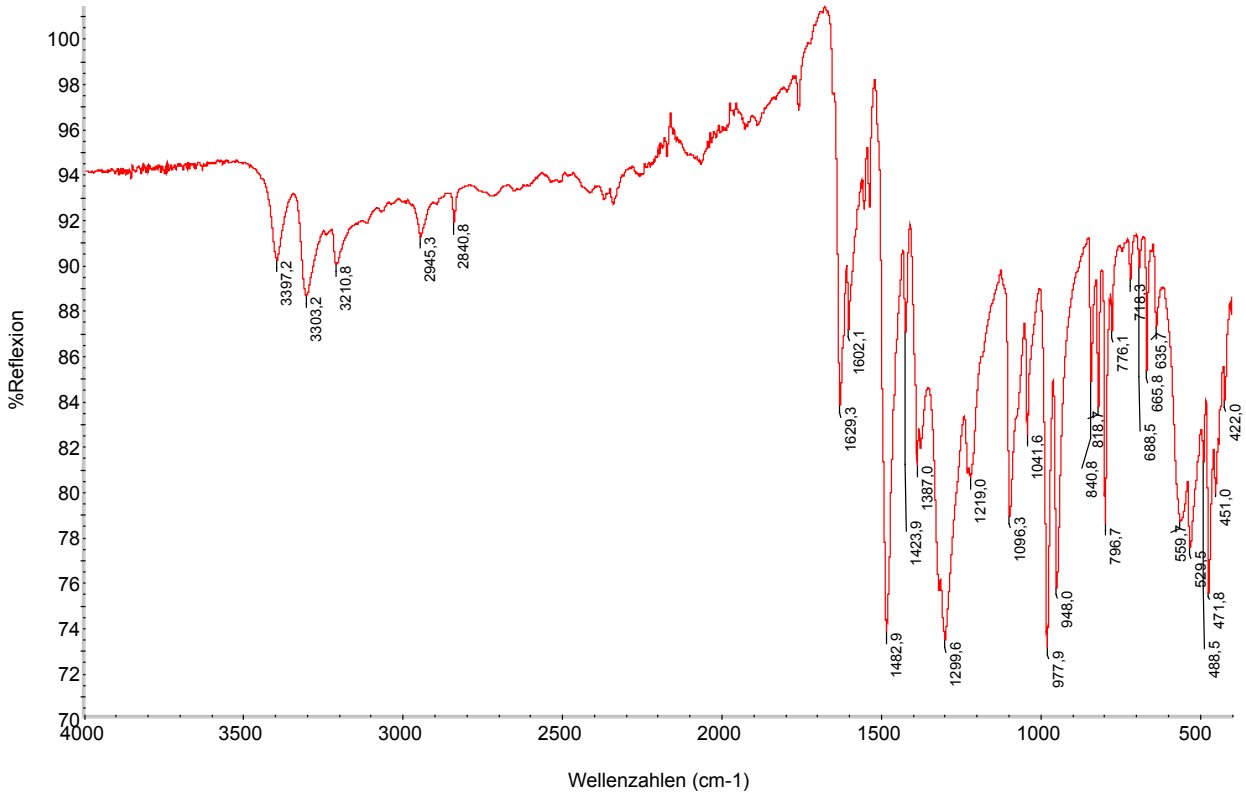

Fig. S 23 Infrared spectra (ATR) of compound **7**.

$[Ag(nfap)CO_2CF_3]_n$ (8):

IR (ATR): $\tilde{\nu}$ = 3327, 3186, 2946, 2820, 1655, 1637, 1610, 1508, 1481, 1426, 1376, 1282, 1189, 1141, 969, 944, 903, 838, 822, 801, 723, 662, 597, 520, 493 cm^{-1}.

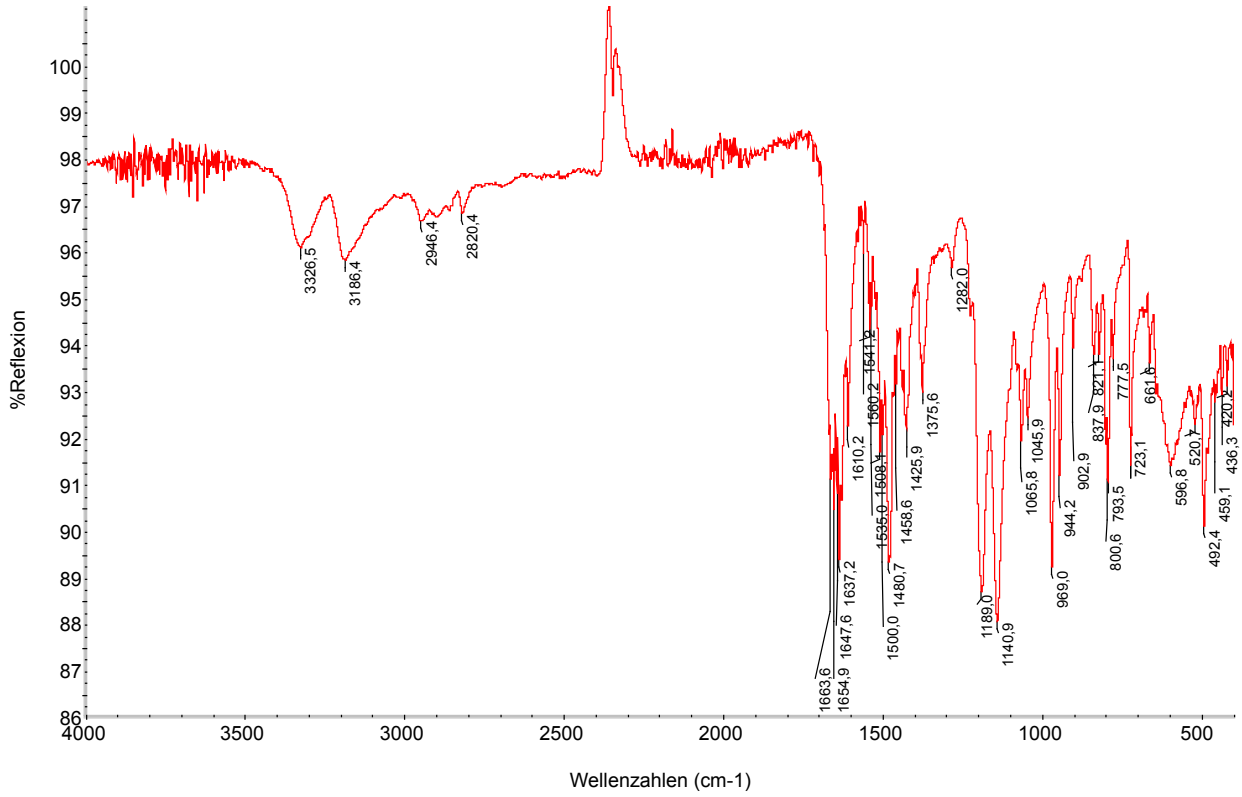

Fig. S 24 Infrared spectra (ATR) of compound **8**.

$[Ag(nfap)SO_3CF_3 \cdot EtOH]_n$ (9):

IR (ATR): $\tilde{\nu}$ = 3394, 3330, 3229, 2942, 2896, 2812, 1642, 1613, 1551, 1500, 1483, 1427, 1375, 1250, 1221, 1168, 1066, 1045, 1025, 974, 953, 920, 794, 760, 634, 558, 509, 491, 419 cm^{-1}.

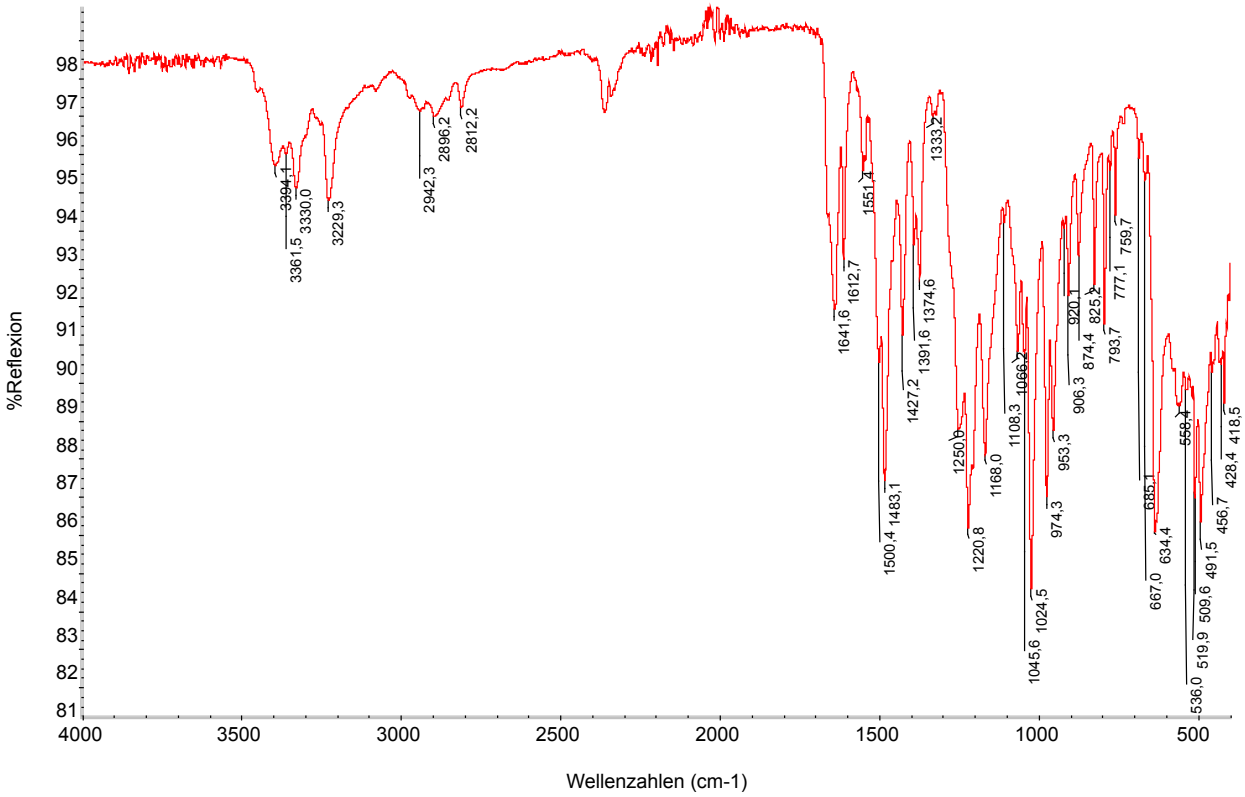

Fig. S 25 Infrared spectra (ATR) of compound **9**.

$[Ag(nfap)ClO_4]_n$ (10):

IR (ATR): $\tilde{\nu}$ = 3456, 3360, 3233, 2942, 2879, 2847, 2808, 1634, 1543, 1504, 1484, 1426, 1373, 1222, 1137, 1049, 970, 943, 920, 793, 618, 470, 433 cm^{-1}.

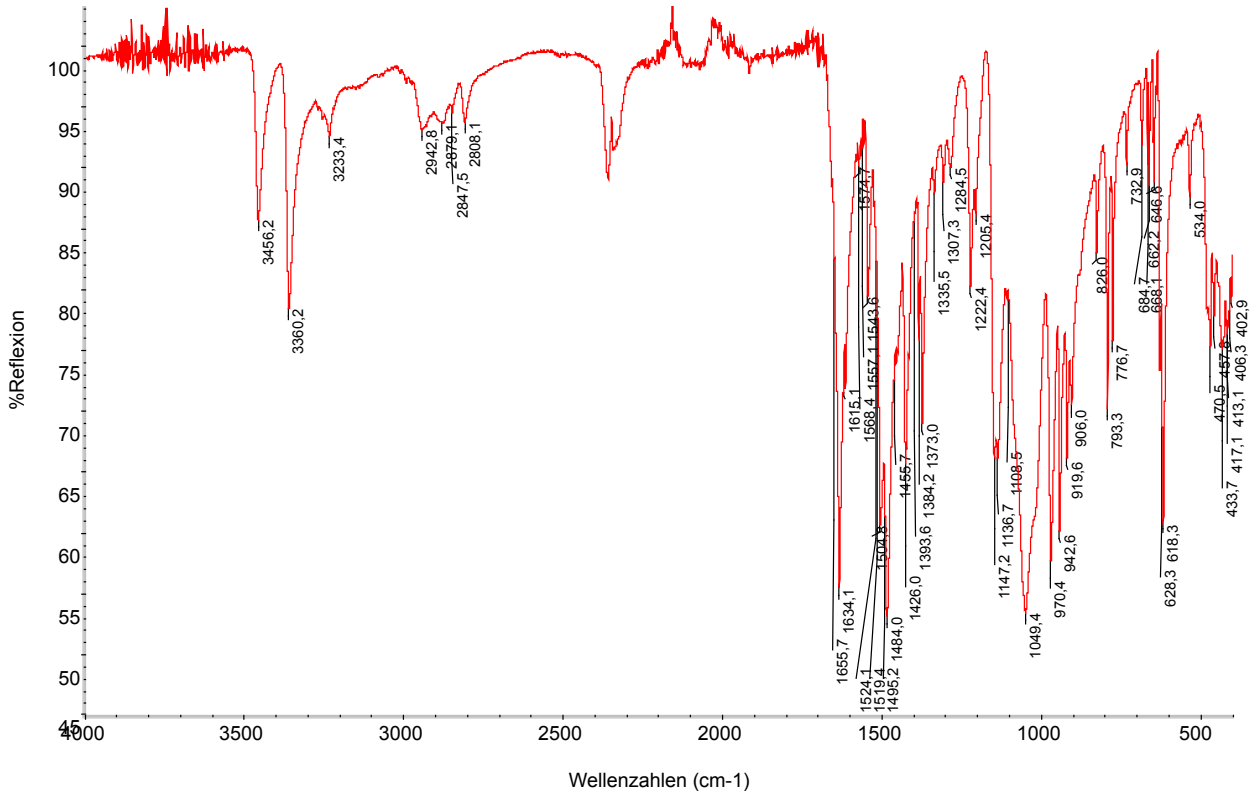

Fig. S 26 Infrared spectra (ATR) of compound **10**.

[Ag(nfap)NO_3]$_n$ (11a):

IR (ATR): = 3383, 3326, 3268, 3226, 2905, 2817, 1648, 1611, 1508, 1478, 1427, 1364, 1319, 1222, 1066, 1045, 967, 942, 793, 776, 669, 545, 488 cm^{-1}.

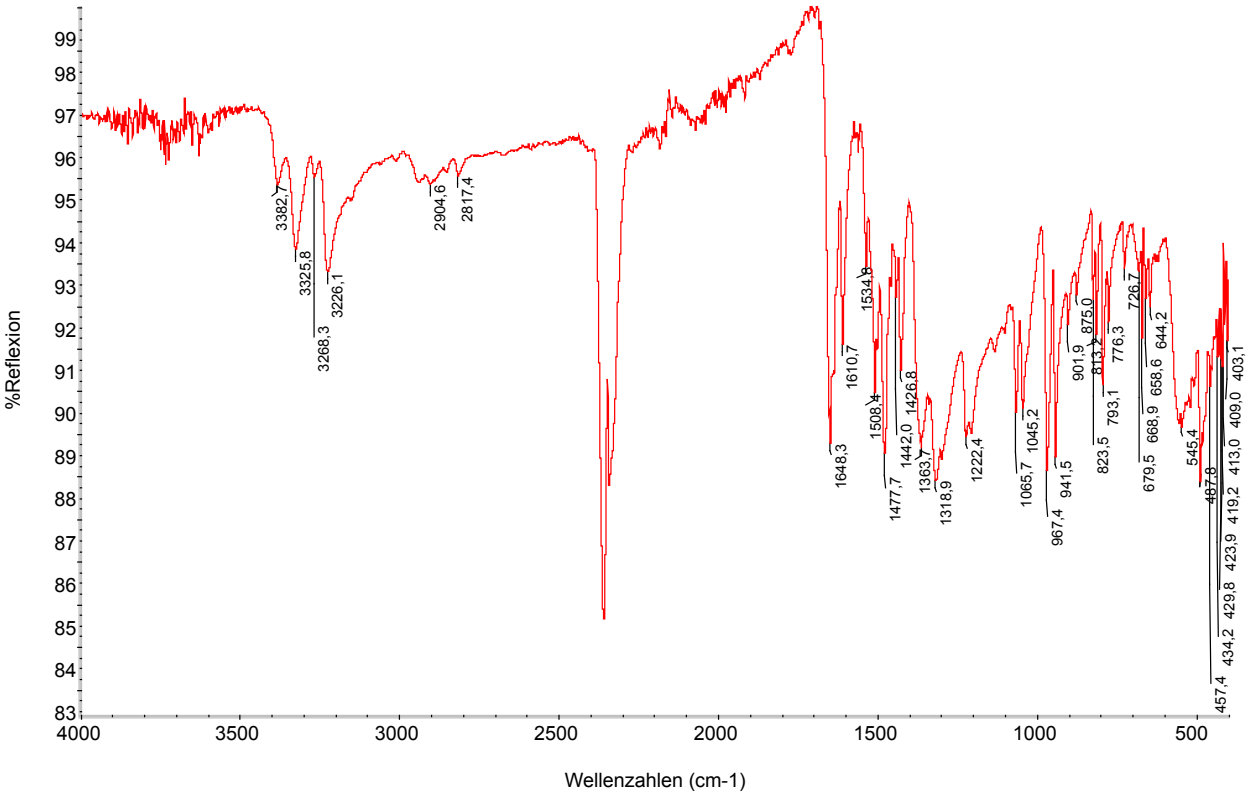

Fig. S 27 Infrared spectra (ATR) of compound **11a**.

$[Ag(nfap)NO_3]_n$ (11b):

IR (ATR): $\tilde{\nu}$ = 3297, 3201, 3057, 2894, 2819, 1639, 1594, 1503, 1486, 1423, 1386, 1277, 1216, 1198, 1065, 1054, 1030, 977, 954, 908, 822, 791, 660, 649, 539, 490, 450, 430 cm^{-1}.

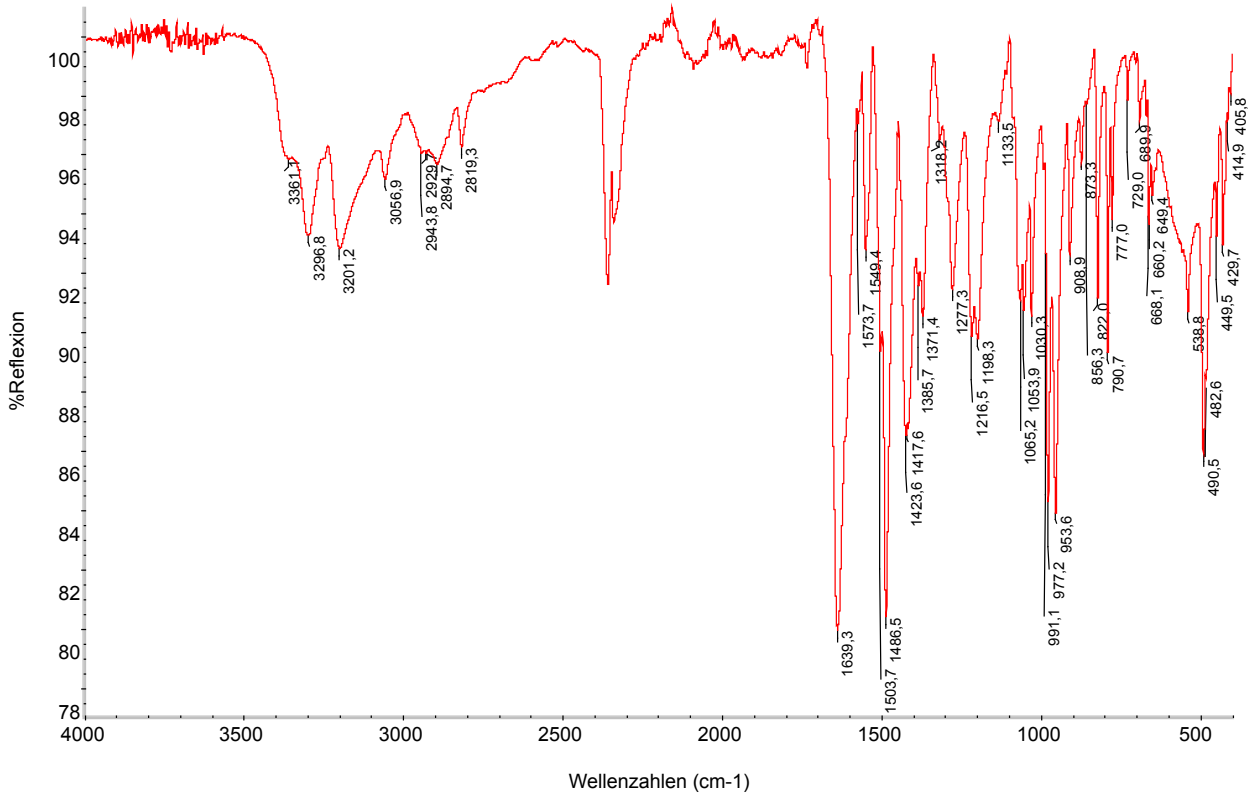

Fig. S 28 Infrared spectra (ATR) of compound **11b**.

PXRD data of the ligands 1 - 3

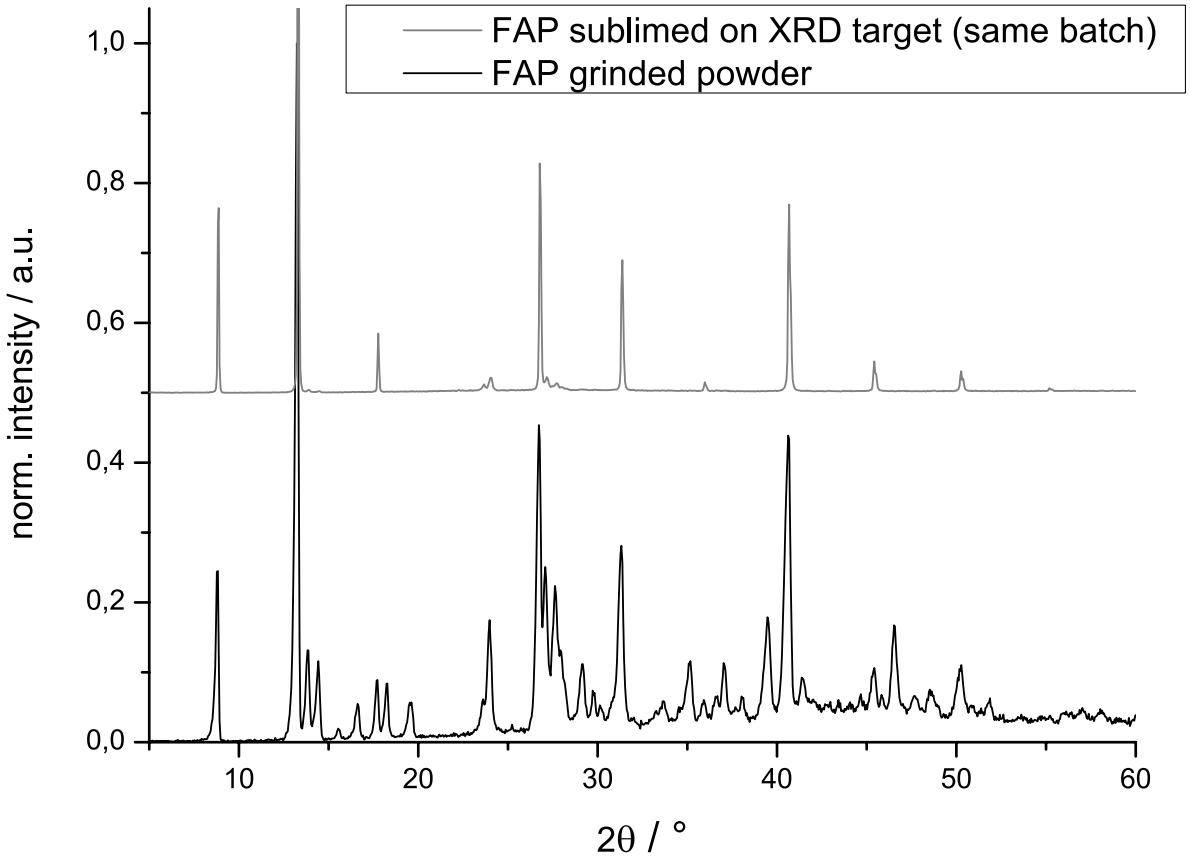

Fig. S 29 FAP XRD spectra. Bottom: measured powder sample (black), top: subl. sample (grey, offset set to +0.50).

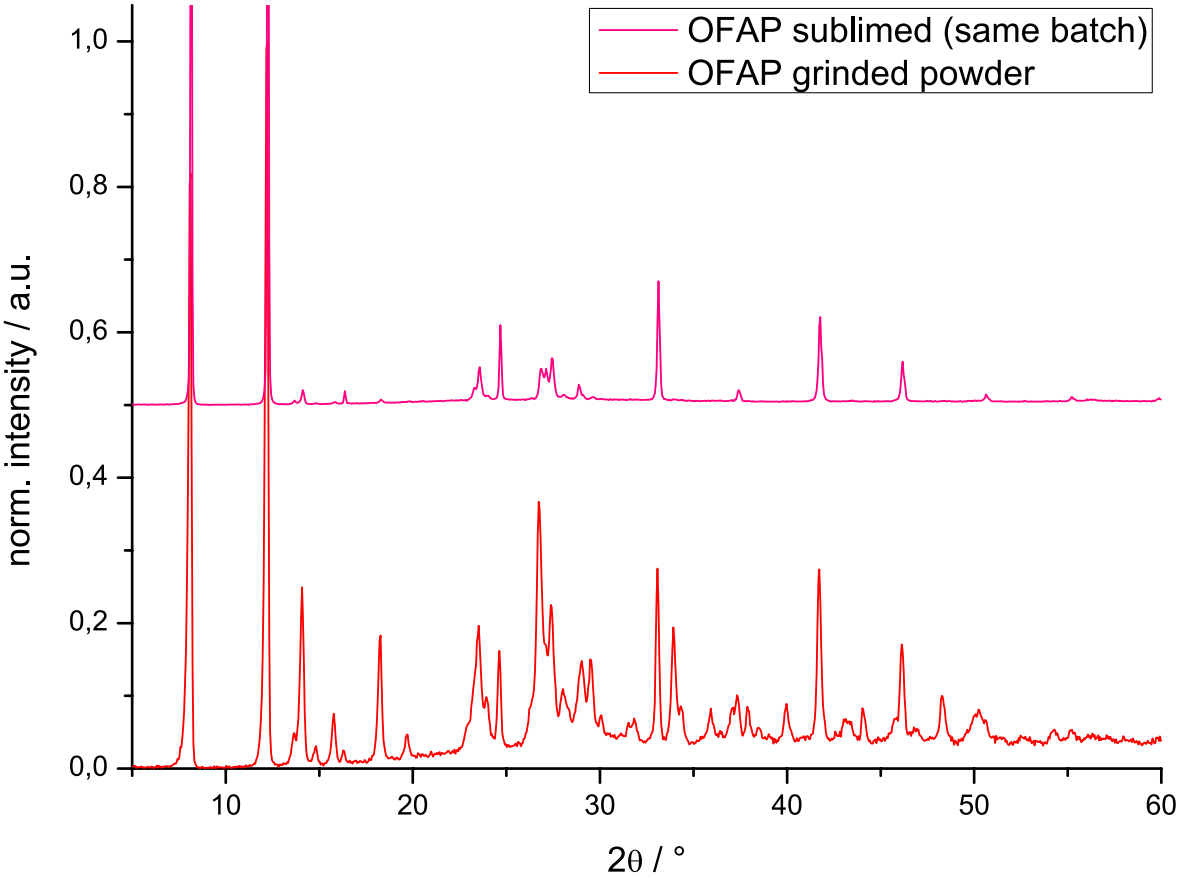

Fig. S 30 OFAP XRD spectra. Bottom: measured powder sample (red), top: subl. sample (magenta, offset set to +0.50).

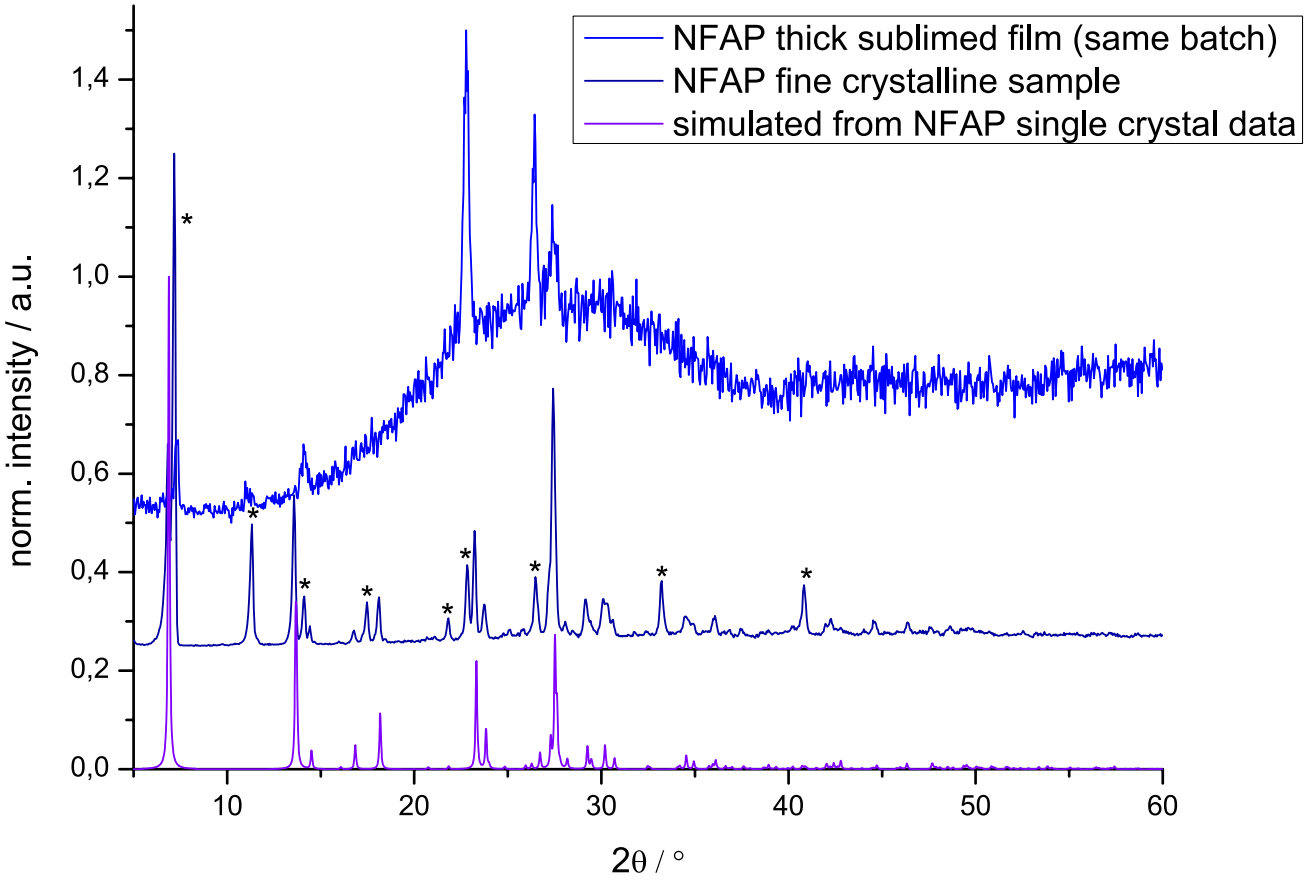

Fig. S 31 NFAP XRD spectra. Bottom simulated spectra for λ = 1.54056 Å (violet), middle: measured powder sample (navy blue, offset set to +0.25), top: subl. sample (blue, offset +0.50).

Additional views on X-ray structures of 4 - 11

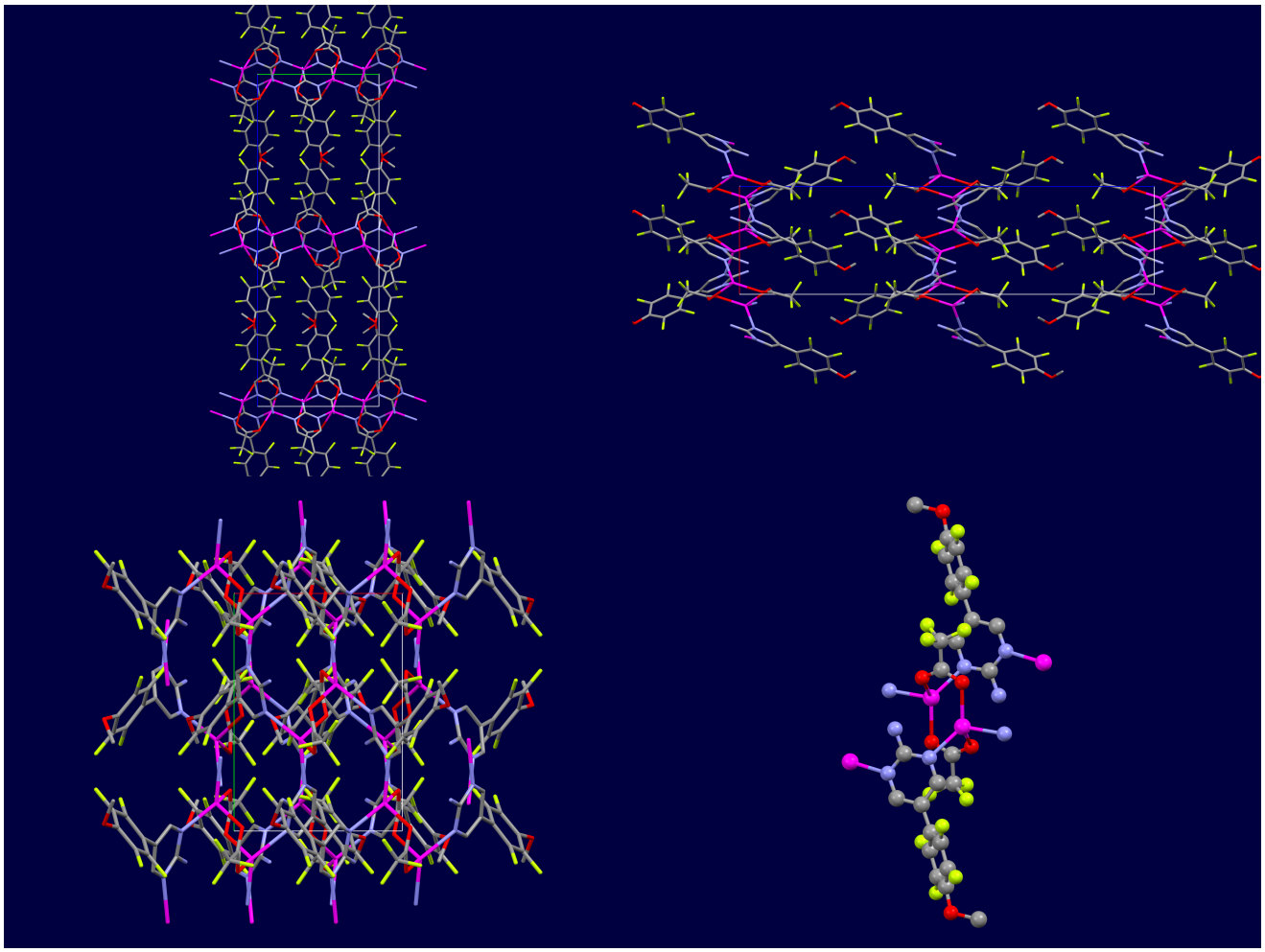

Fig. S 32 View on unit cell along *a* axis (top left), *b* axis (top right), and *c* axis (bottom left) and random view to emphasize structure details (bottom right) of $[Ag(ofap)CO_2CF_3]_n$ (**4**)

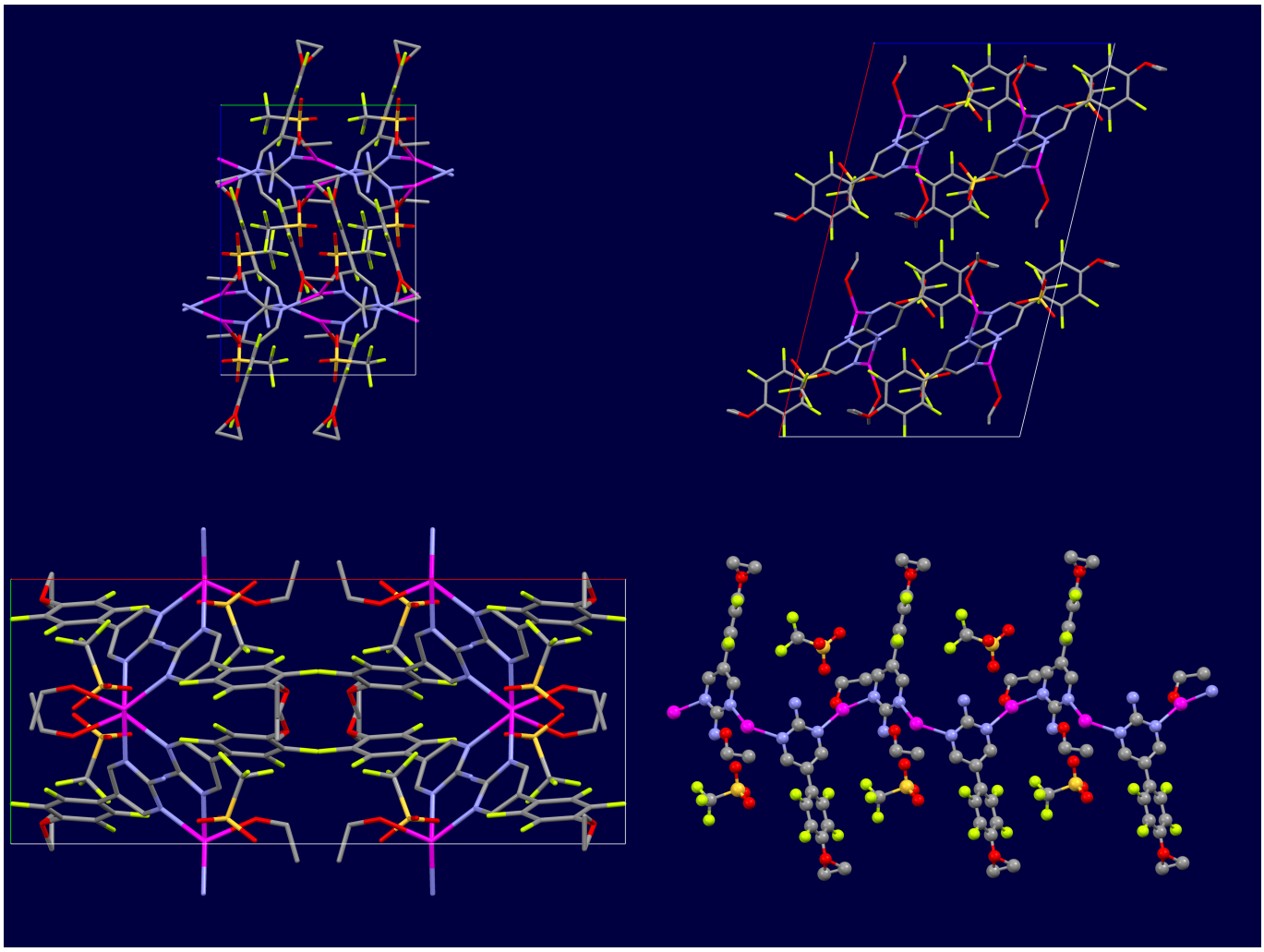

Fig. S 33 View on unit cell along *a* axis (top left), *b* axis (top right), and *c* axis (bottom left) and random view to emphasize structure details (bottom right) of $[Ag(ofap)SO_3CF_3 \cdot EtOH]_n$ (**5**)

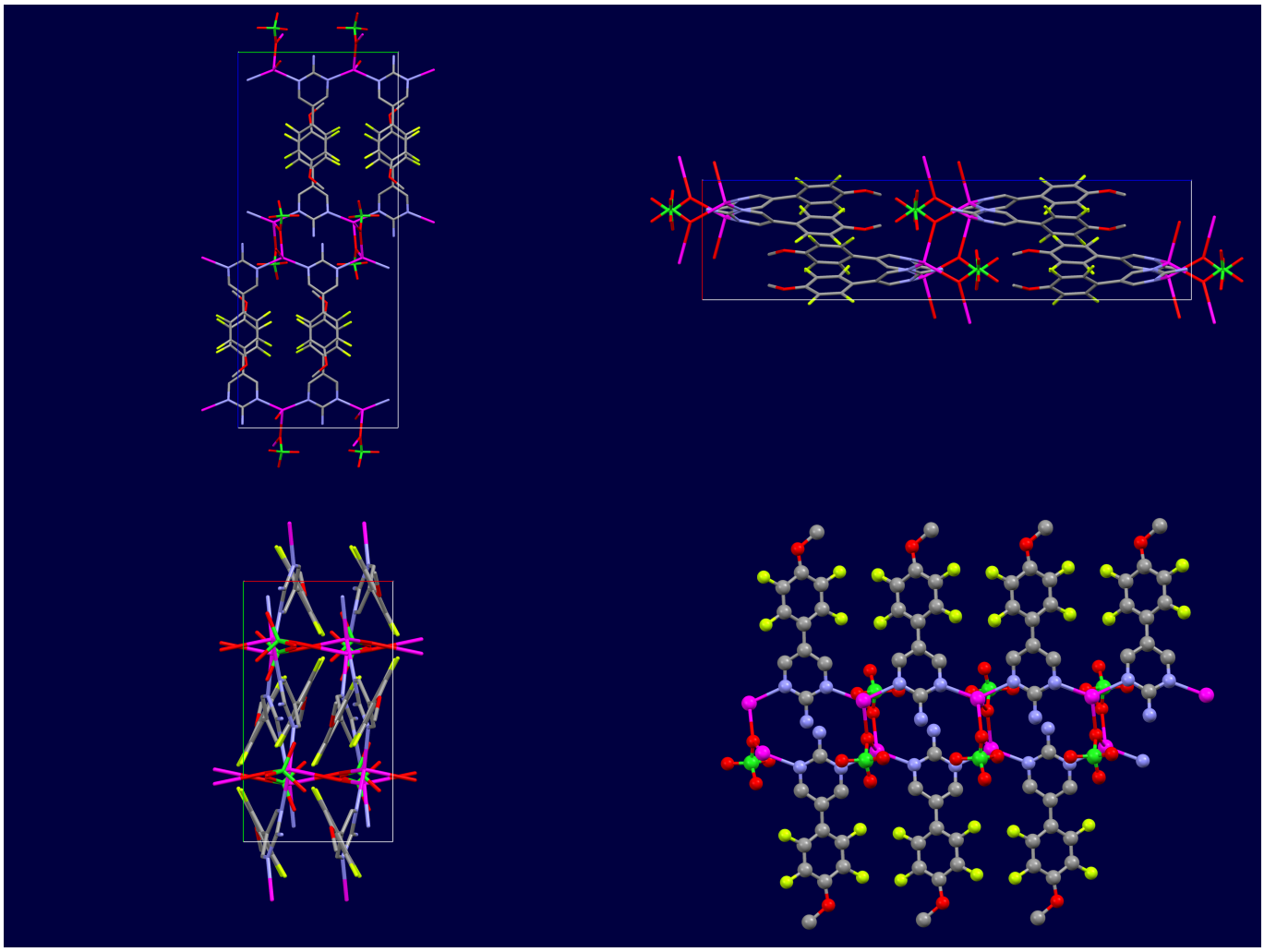

Fig. S 34 View on unit cell along *a* axis (top left), *b* axis (top right), and *c* axis (bottom left) and random view to emphasize structure details (bottom right) of $[Ag(ofap)ClO_4]_n$ (**6**)

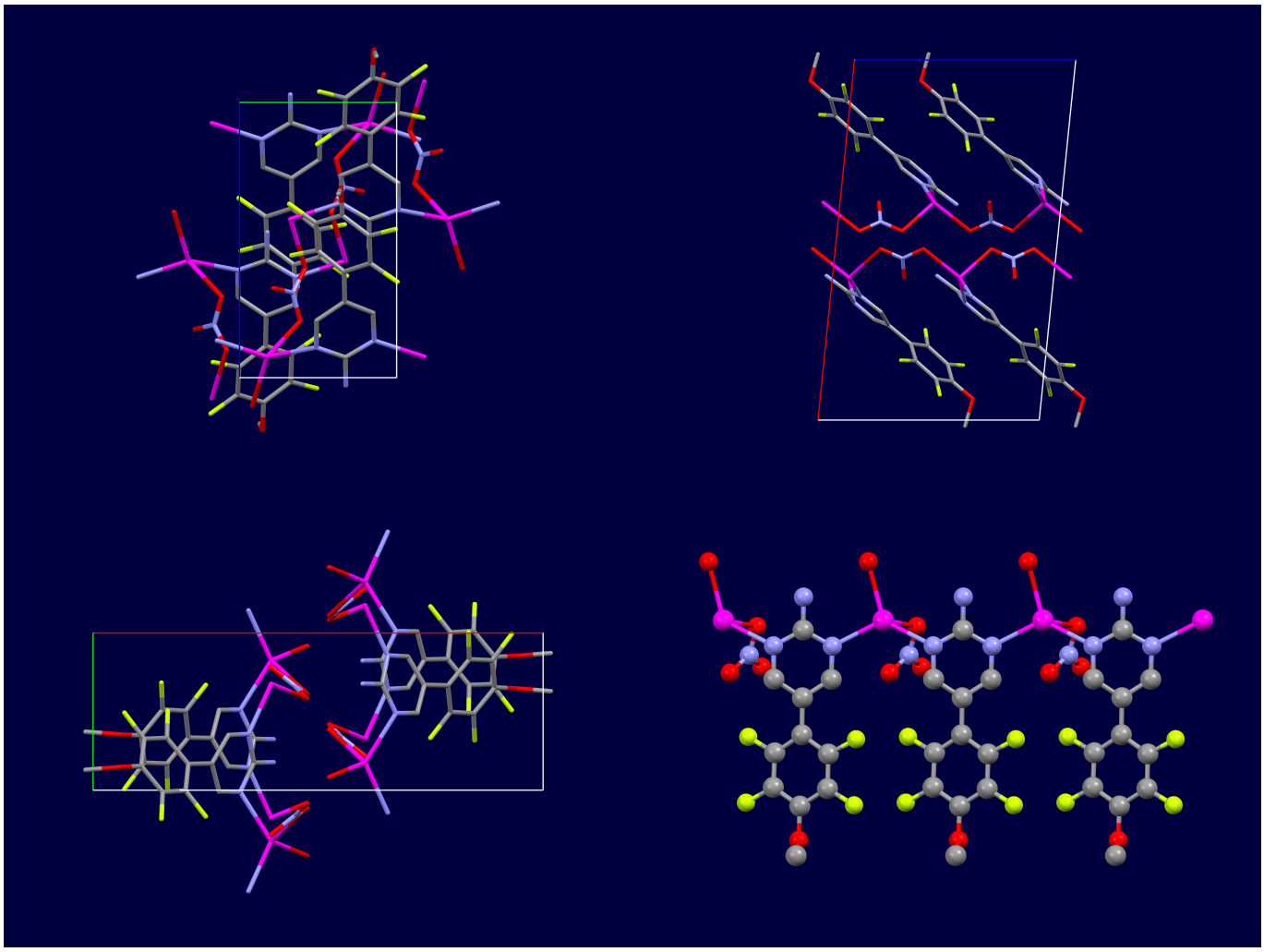

Fig. S 35 View on unit cell along *a* axis (top left), *b* axis (top right), and *c* axis (bottom left) and random view to emphasize structure details (bottom right) of $[Ag(ofap)NO_3]]_n$ (**7**)

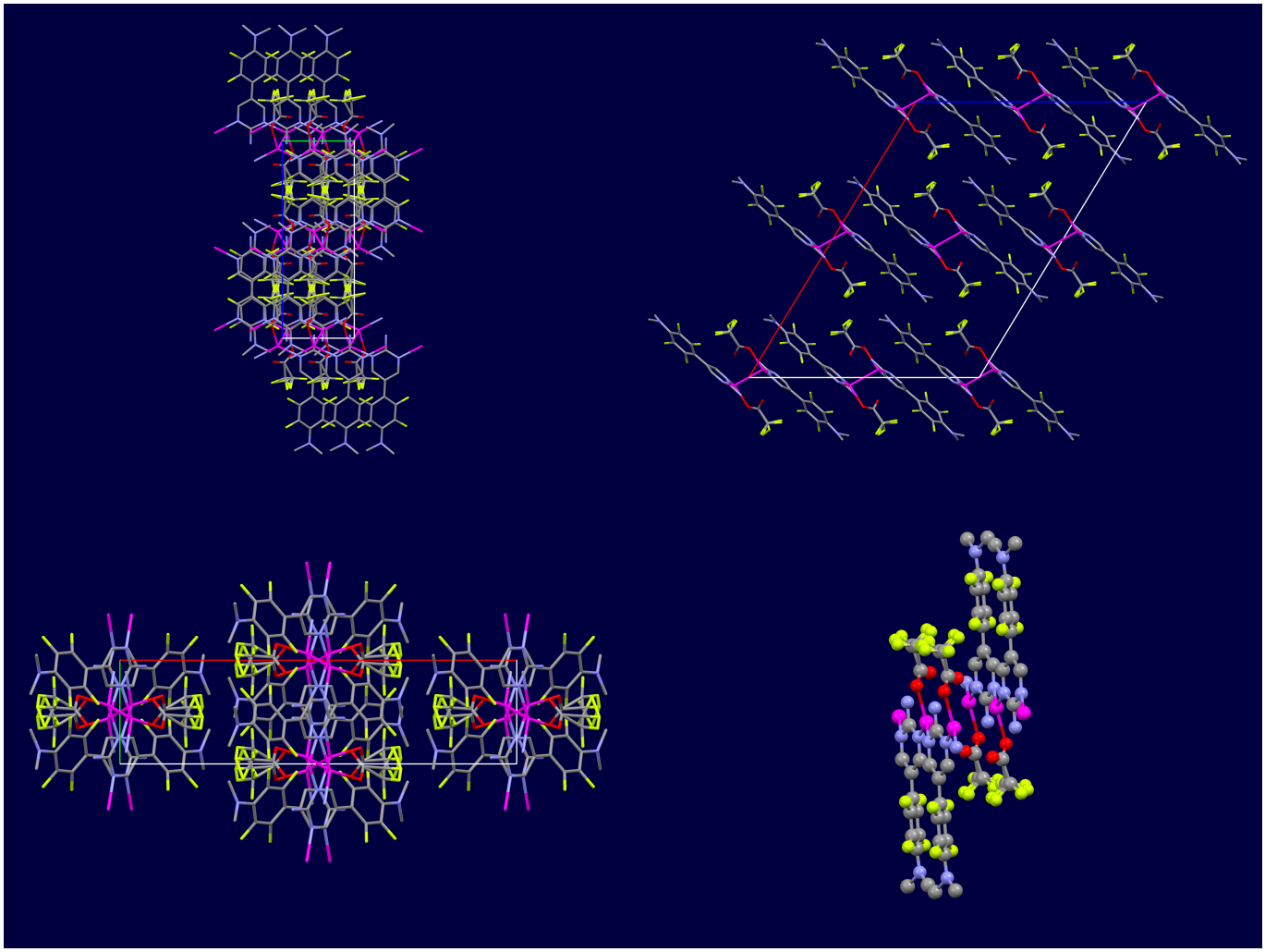

Fig. S 36 View on unit cell along *a* axis (top left), *b* axis (top right), and *c* axis (bottom left) and random view to emphasize structure details (bottom right) of $[Ag(nfap)CO_2CF_3]_n$ (**8**)

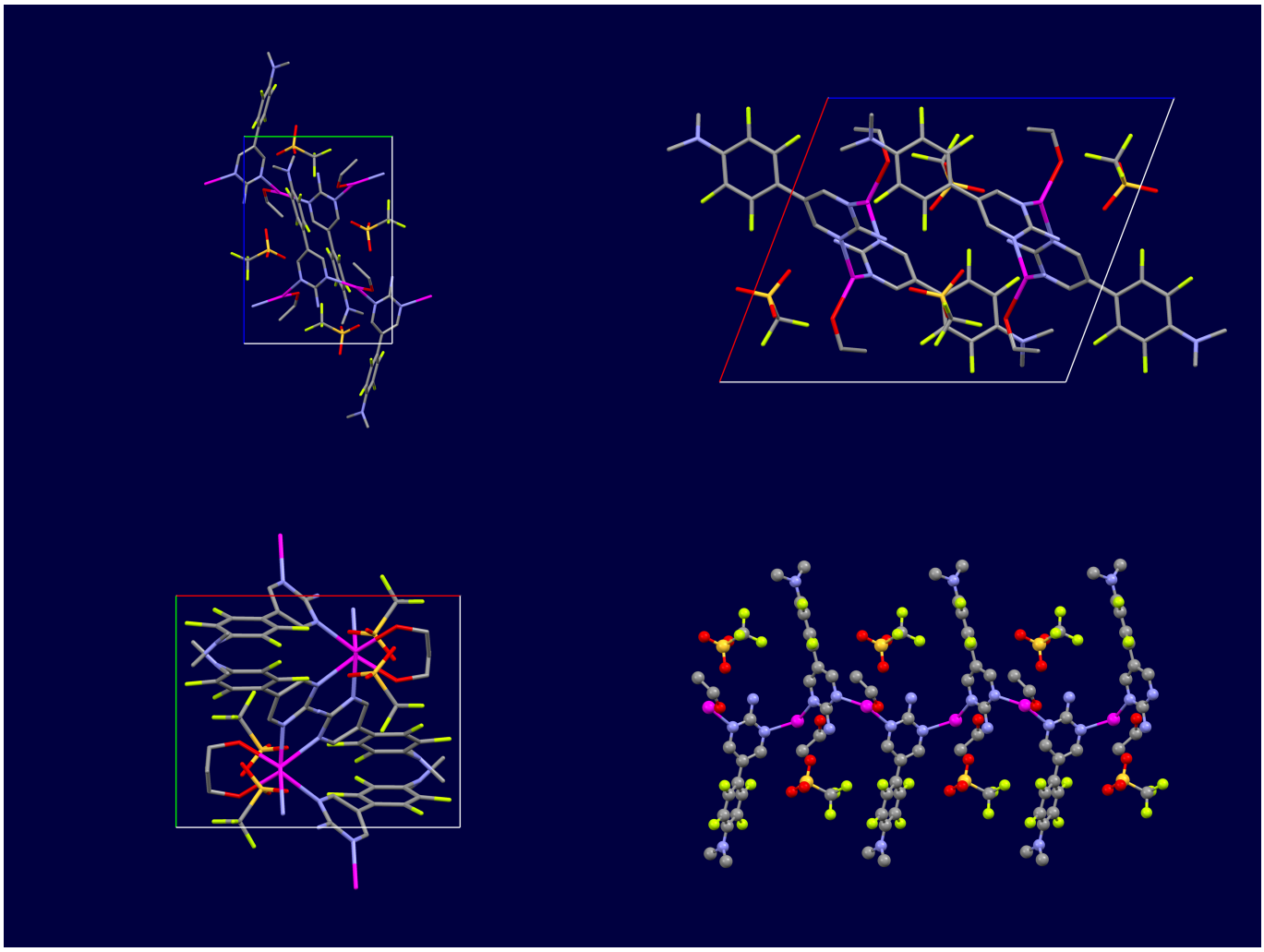

Fig. S 37 View on unit cell along *a* axis (top left), *b* axis (top right), and *c* axis (bottom left) and random view to emphasize structure details (bottom right) of $[Ag(nfap)SO_3CF_3 \cdot EtOH]_n$ (**9**)

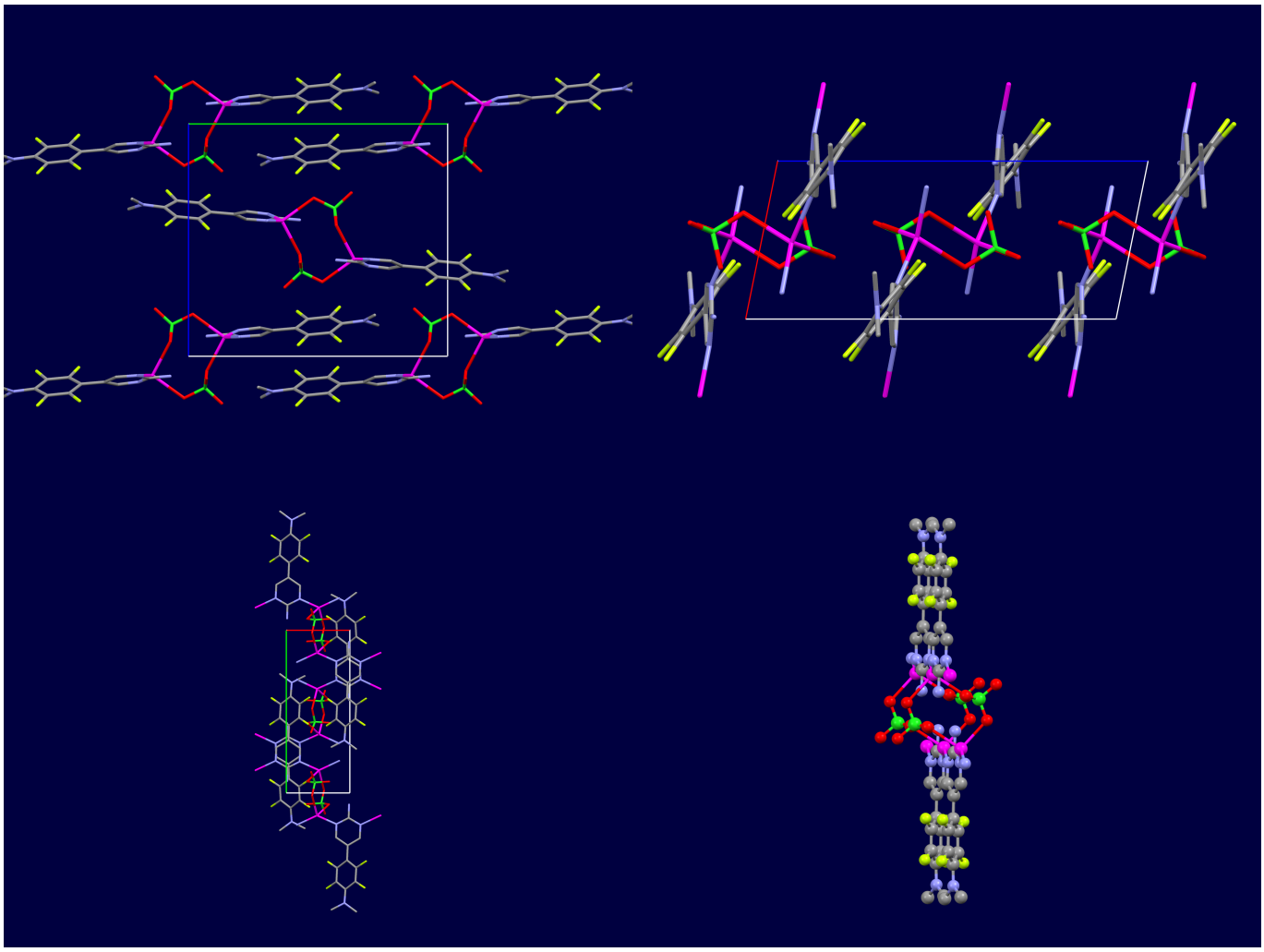

Fig. S 38 View on unit cell along *a* axis (top left), *b* axis (top right), and *c* axis (bottom left) and random view to emphasize structure details (bottom right) of $[Ag(nfap)ClO_4]_n$ (**10**)

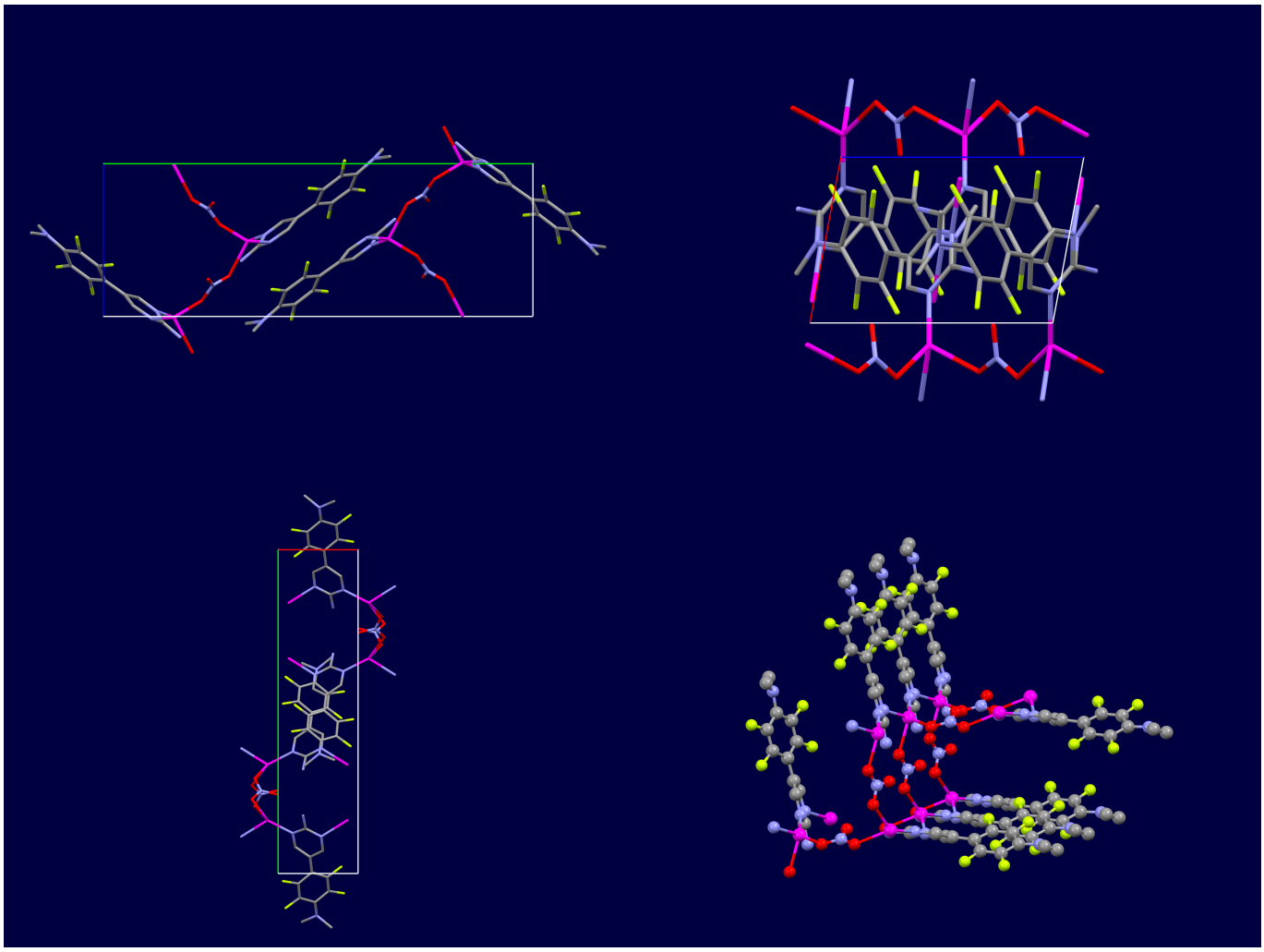

Fig. S 39 View on unit cell along *a* axis (top left), *b* axis (top right), and *c* axis (bottom left) and random view to emphasize structure details (bottom right) of $[Ag(nfap)NO_3]_n$ (**11a**)

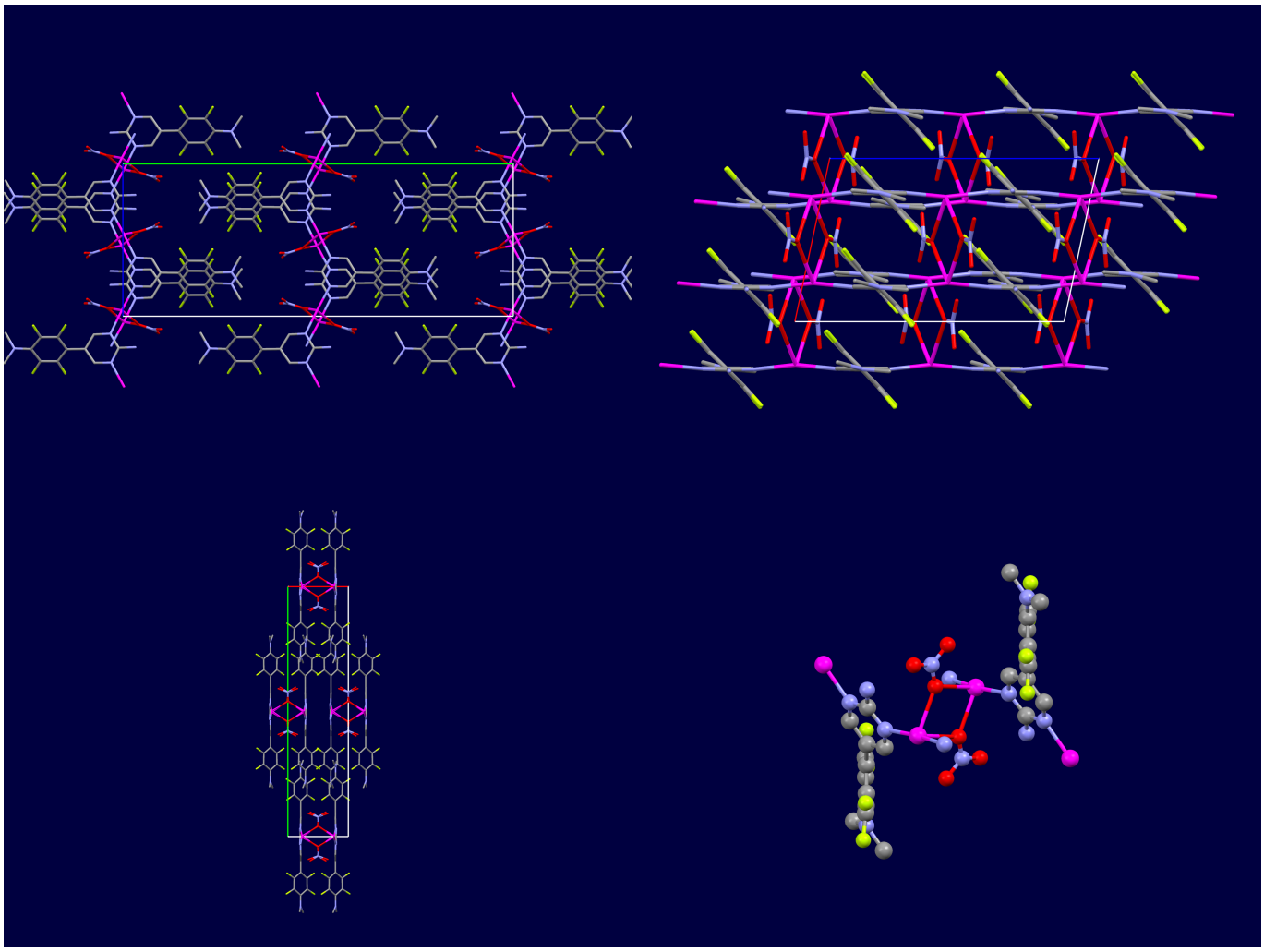

Fig. S 40 View on unit cell along *a* axis (top left), *b* axis (top right), and *c* axis (bottom left) and random view to emphasize structure details (bottom right) of $[Ag(nfap)NO_3]_n$ (**11b**)

Statistics of Table 4 in the manuscript

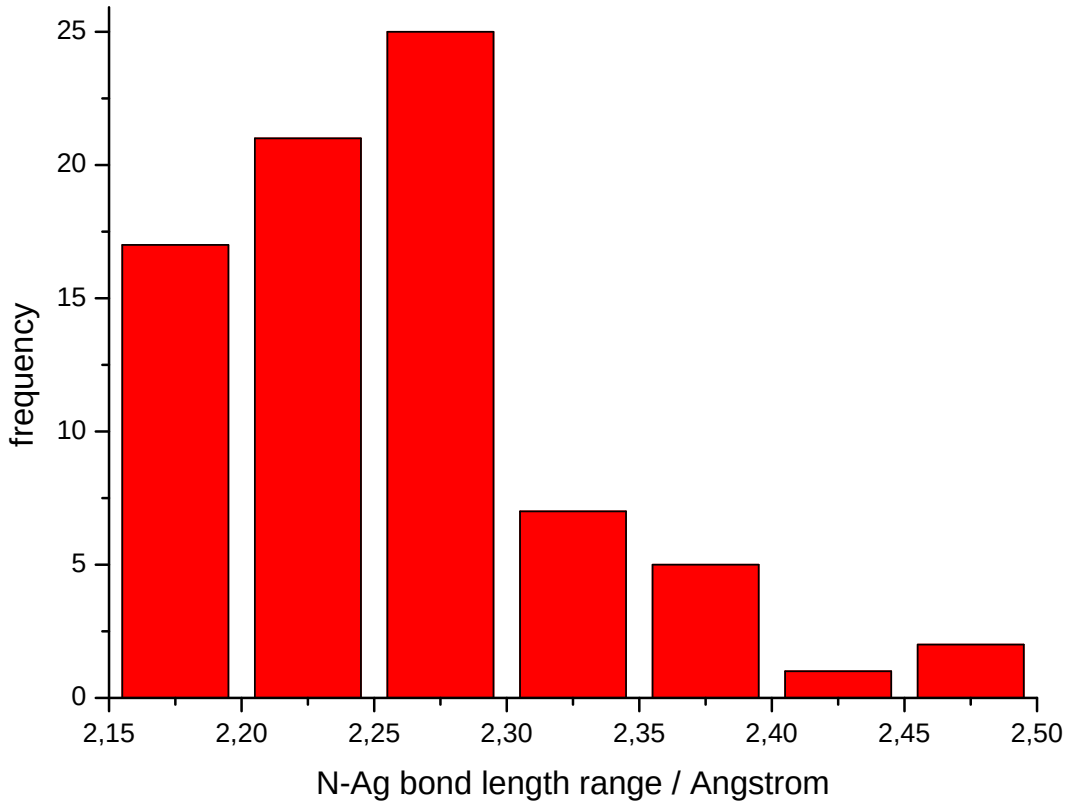

Fig. S 41 Histogram for bond length N–Ag in AP Ag^{I} coordination polymers.

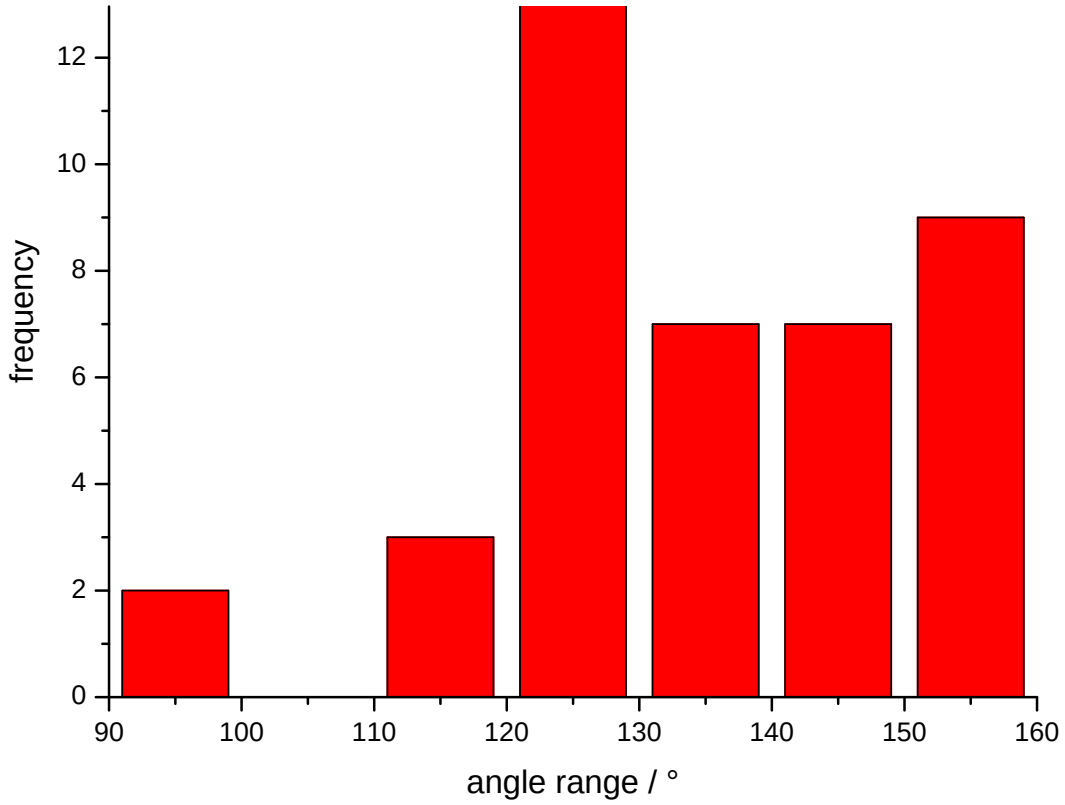

Fig. S 42 Histogram for N–Ag–N angle in AP Ag^{I} coordination polymers.

References

[1] P. W. Wigler, *Biochemistry*, 1965, **4**, 1667–1670.

[2] L. Weber, J. Kahlert, R. Brockhinke, L. Böhling, A. Brockhinke, H.-G. Stammler, B. Neumann, R. A. Harder and M. A. Fox, *Chem. – Eur. J.*, 2012, **18**, 8347–8357.

[3] I. Stoll, R. Brockhinke, A. Brockhinke, M. Böttcher, T. Koop, H.-G. Stammler, B. Neumann, A. Niemeyer, A. Hütten and J. Mattay, *Chem. Mater.*, 2010, **22**, 4749–4755.

[4] J. G. Contreras, G. V. Seguel and J. A. Gnecco, *Spectrochim. Acta, Part A*, 1992, **48**, 525–532.

[5] S. Akyuz, *J. Supramol. Chem.*, 2002, **2**, 401–404.

[6] D. Kovala-Demertzi, N. Kourkoumelis, P. Tavridou, A. Moukarika, P. D. Akrivos and U. Russo, *Spectrochim. Acta, Part A*, 1998, **54**, 1801–1809.

[7] J.-P. Charland and A. L. Beauchamp, *J. Chem. Crystallogr.*, 1985, **15**, 581–601.

[8] G. Smith, B. A. Cloutt, D. E. Lynch, K. A. Byriel and C. H. L. Kennard, *Inorg. Chem.*, 1998, **37**, 3236–3242.

[9] S. M. Holmes, S. G. Mckinley and G. S. Girolami, *Inorganic Syntheses*, John Wiley & Sons, Inc., 2002, vol. 33, ch. 2, pp. 91–103.

[10] (*a*) A. I. Boltalin, E. V. Karpova, Y. M. Korenev and V. A. Sipachev, *J. Mol. Struct.*, 2002, **643**, 161–169; (*b*) M. J. Baillie, D. H. Brown, K. C. Moss and D. W. A. Sharp, *J. Chem. Soc. A*, 1968, 3110–3114.

[11] (*a*) D. H. Johnston and D. F. Shriver, *Inorg. Chem.*, 1993, **32**, 1045–1047; (*b*) S. P. Gejji, K. Hermansson and J. Lindgren, *J. Phys. Chem*, 1993, **97**, 3712–3715.

[12] G. Ritzhaupt and J. P. Devlin, *J. Chem. Phys.*, 1975, **62**, 1982–1986.

[13] (*a*) F. A. Miller and C. H. Wilkins, *Anal. Chem.*, 1952, **24**, 1253–1294; (*b*) F. A. Miller, G. L. Carlson, F. F. Bentley and W. H. Jones, *Spectrochim. Acta*, 1960, **16**, 135–235.

[14] H. D. Lutz, R. A. Becker, W. Eckers, B. G. Hölscher and H. J. Berthold, *Spectrochim. Acta, Part A*, 1983, **39**, 7–14.

[15] R. Frech and J. P. Manning, *Electrochim. Acta*, 1992, **37**, 1499–1503.

[16] C. C. Addison and B. M. Gatehouse, *J. Chem. Soc.*, 1960, 613–616.

[17] F. Vratny, *Appl. Spectrosc.*, 1959, **13**, 59–70.

[18] A. B. P. Lever, E. Mantovani and B. S. Ramaswamy, *Can. J. Chem.*, 1971, **49**, 1957–1964.

[19] M. J. Frisch, G. W. Trucks, H. B. Schlegel, G. E. Scuseria, M. A. Robb, J. R. Cheeseman, G. Scalmani, V. Barone, B. Mennucci, G. A. Petersson, H. Nakatsuji, M. Caricato, X. Li, H. P. Hratchian, A. F. Izmaylov, J. Bloino, G. Zheng, J. L. Sonnenberg, M. Hada, M. Ehara, K. Toyota, R. Fukuda, J. Hasegawa, M. Ishida, T. Nakajima, Y. Honda, O. Kitao, H. Nakai, T. Vreven, J. A. Montgomery, Jr., J. E. Peralta, F. Ogliaro, M. Bearpark, J. J. Heyd, E. Brothers, K. N. Kudin, V. N. Staroverov, R. Kobayashi, J. Normand, K. Raghavachari, A. Rendell, J. C. Burant, S. S. Iyengar, J. Tomasi, M. Cossi, N. Rega, J. M. Millam, M. Klene, J. E. Knox, J. B. Cross, V. Bakken, C. Adamo, J. Jaramillo, R. Gomperts, R. E. Stratmann, O. Yazyev, A. J. Austin, R. Cammi, C. Pomelli, J. W. Ochterski, R. L. Martin, K. Morokuma, V. G. Zakrzewski, G. A. Voth, P. Salvador, J. J. Dannenberg, S. Dapprich, A. D. Daniels, O. Farkas, J. B. Foresman, J. V. Ortiz, J. Cioslowski and D. J. Fox, *Gaussian 09 Revision A.1*, 2009, Gaussian, Inc., Wallingford, CT, USA.